AD_____

MIPR NO: 94MM4539

TITLE: Crystal Diffraction Spectrometry for Accurate, Non-Invasive KV/Spectral Measurement for Improvement of Mammographic Image Quality

PRINCIPAL INVESTIGATOR(S): Richard D. Deslattes, Ph.D.
Lawrence T. Hudson, Ph.D.

CONTRACTING ORGANIZATION: National Institute of Standards and Technology
Gaithersburg, Maryland 20899

REPORT DATE: December 1996

TYPE OF REPORT: Final

PREPARED FOR: U.S. Army Medical Research and Materiel Command
Fort Detrick, Frederick, Maryland 21702-5012

REPORT DOCUMENTATION PAGE

Form Approved
OMB No. 0704-0188

1. AGENCY USE ONLY (Leave blank)	2. REPORT DATE	3. REPORT TYPE AND DATES COVERED
	December 1996	Final Report (18 Apr 94 - 31 Dec 96)

4. TITLE AND SUBTITLE
Crystal Diffraction Spectrometry for Accurate, Non-Invasive KV/Spectral Measurement for Improvement of Mammographic Image Quality

5. FUNDING NUMBERS
94MM4539

6. AUTHOR(S)
Richard D. Deslattes, Ph.D.
Lawrence T. Hudson, Ph.D.

7. PERFORMING ORGANIZATION NAME(S) AND ADDRESS(ES)
National Institute of Standards and Technology
Gaithersburg, Maryland 20899

8. PERFORMING ORGANIZATION REPORT NUMBER

9. SPONSORING/MONITORING AGENCY NAME(S) AND ADDRESS(ES)
U.S. Army Medical Research and Material Command
Fort Detrick
Frederick, Maryland 21702-5012

10. SPONSORING/MONITORING AGENCY REPORT NUMBER

11. SUPPLEMENTARY NOTES

12a. DISTRIBUTION/AVAILABILITY STATEMENT
Approved for public release; distribution unlimited

12b. DISTRIBUTION CODE

13. ABSTRACT *(Maximum 200 words)*

This contract has been devoted to the development and demonstration of the NIST prototype crystal spectrometer which was designed to provide accurate measurement of x-ray source voltage and full spectral characterization of the radiation emitted from mammographic x-ray sources. A major advance has been the movement from film to solid state image registration. Studies in a clinical environment led to refinements in packaging and portability, and revealed the need to increase device sensitivity. The detection efficiency was increased manyfold by optimum choice of diffracting crystal plane and modification of the CCD sensor package. The significance of these advances is that we now have an instrument which: measures kVp to an accuracy in excess of clinical requirements, is easily adaptable to the clinical setting, records the entire spectral profile, including the effects of both inherent and added filtration, and is sensitive enough to obtain these data within the time of a typical mammographic exposure. Not only will this contribute to the quality control of mammography but potentially to refinements in technique. During the contractual period, technology transfer of the mammographic spectrometer was brought to the stage of commercial manufacture.

14. SUBJECT TERMS	15. NUMBER OF PAGES
curved crystal spectrometry, diffraction, high voltage, mammography, x-rays	40
	16. PRICE CODE

17. SECURITY CLASSIFICATION OF REPORT	18. SECURITY CLASSIFICATION OF THIS PAGE	19. SECURITY CLASSIFICATION OF ABSTRACT	20. LIMITATION OF ABSTRACT
Unclassified	Unclassified	Unclassified	Unlimited

GENERAL INSTRUCTIONS FOR COMPLETING SF 298

The Report Documentation Page (RDP) is used in announcing and cataloging reports. It is important that this information be consistent with the rest of the report, particularly the cover and title page. Instructions for filling in each block of the form follow. It is important to *stay within the lines* to meet *optical scanning requirements*.

Block 1. Agency Use Only *(Leave blank)*.

Block 2. Report Date. Full publication date including day, month, and year, if available (e.g. 1 Jan 88). Must cite at least the year.

Block 3. Type of Report and Dates Covered. State whether report is interim, final, etc. If applicable, enter inclusive report dates (e.g. 10 Jun 87 - 30 Jun 88).

Block 4. Title and Subtitle. A title is taken from the part of the report that provides the most meaningful and complete information. When a report is prepared in more than one volume, repeat the primary title, add volume number, and include subtitle for the specific volume. On classified documents enter the title classification in parentheses.

Block 5. Funding Numbers. To include contract and grant numbers; may include program element number(s), project number(s), task number(s), and work unit number(s). Use the following labels:

C	- Contract	PR	- Project
G	- Grant	TA	- Task
PE	- Program Element	WU	- Work Unit Accession No.

Block 6. Author(s). Name(s) of person(s) responsible for writing the report, performing the research, or credited with the content of the report. If editor or compiler, this should follow the name(s).

Block 7. Performing Organization Name(s) and Address(es). Self-explanatory.

Block 8. Performing Organization Report Number. Enter the unique alphanumeric report number(s) assigned by the organization performing the report.

Block 9. Sponsoring/Monitoring Agency Name(s) and Address(es). Self-explanatory.

Block 10. Sponsoring/Monitoring Agency Report Number. *(If known)*

Block 11. Supplementary Notes. Enter information not included elsewhere such as: Prepared in cooperation with...; Trans. of...; To be published in.... When a report is revised, include a statement whether the new report supersedes or supplements the older report.

Block 12a. Distribution/Availability Statement. Denotes public availability or limitations. Cite any availability to the public. Enter additional limitations or special markings in all capitals (e.g. NOFORN, REL, ITAR).

- DOD - See DoDD 5230.24, "Distribution Statements on Technical Documents."
- DOE - See authorities.
- NASA - See Handbook NHB 2200.2.
- NTIS - Leave blank.

Block 12b. Distribution Code.

- DOD - Leave blank.
- DOE - Enter DOE distribution categories from the Standard Distribution for Unclassified Scientific and Technical Reports.
- NASA - Leave blank.
- NTIS - Leave blank.

Block 13. Abstract. Include a brief *(Maximum 200 words)* factual summary of the most significant information contained in the report.

Block 14. Subject Terms. Keywords or phrases identifying major subjects in the report.

Block 15. Number of Pages. Enter the total number of pages.

Block 16. Price Code. Enter appropriate price code *(NTIS only)*.

Blocks 17. - 19. Security Classifications. Self-explanatory. Enter U.S. Security Classification in accordance with U.S. Security Regulations (i.e., UNCLASSIFIED). If form contains classified information, stamp classification on the top and bottom of the page.

Block 20. Limitation of Abstract. This block must be completed to assign a limitation to the abstract. Enter either UL (unlimited) or SAR (same as report). An entry in this block is necessary if the abstract is to be limited. If blank, the abstract is assumed to be unlimited.

★U.S.GPO:1991-0-299-935

FOREWORD

Opinions, interpretations, conclusions and recommendations are those of the author and are not necessarily endorsed by the US Army.

____ Where copyrighted material is quoted, permission has been obtained to use such material.

____ Where material from documents designated for limited distribution is quoted, permission has been obtained to use the material.

RDD Citations of commercial organizations and trade names in this report do not constitute an official Department of Army endorsement or approval of the products or services of these organizations.

____ In conducting research using animals, the investigator(s) adhered to the "Guide for the Care and Use of Laboratory Animals," prepared by the Committee on Care and Use of Laboratory Animals of the Institute of Laboratory Resources, National Research Council (NIH Publication No. 86-23, Revised 1985).

____ For the protection of human subjects, the investigator(s) adhered to policies of applicable Federal Law 45 CFR 46.

____ In conducting research utilizing recombinant DNA technology, the investigator(s) adhered to current guidelines promulgated by the National Institutes of Health.

____ In the conduct of research utilizing recombinant DNA, the investigator(s) adhered to the NIH Guidelines for Research Involving Recombinant DNA Molecules.

____ In the conduct of research involving hazardous organisms, the investigator(s) adhered to the CDC-NIH Guide for Biosafety in Microbiological and Biomedical Laboratories.

R.D. Delather 12/5/96

PI - Signature Date

TABLE OF CONTENTS

Introduction

Nature of the Problem. This work was motivated by a series of letters to the Director of NIST asking for assistance with high-voltage standardization for mammography. It is well established that the mammographic image quality is sensitive to the high voltage (kV) applied to the x-ray source. Clinical experience indicates that changes as small as 1 kV are significant [1]. Less frequently discussed, though also clearly important, is the overall spectral distribution of the radiation delivered to the patient. Recent work in the Physics Laboratory at the National Institute of Standards and Technology (NIST), has resulted in prototype instruments based on (Bragg-Laue) crystal diffraction to gain accurate measurement of x-ray source voltage and full spectral characterization of the emitted radiation. This work has been disseminated in several archival publications [2,3,21] describing the metrological problems which were overcome. The approaches to kV standardization used prior to the recent NIST work in the mammographic energy regime possess inherent limitations as discussed below.

Although traditional, 'invasive' (with respect to the power source) high-voltage divider technique offers adequate accuracy for the case of well-filtered DC potentials, problems arise from the limited accessibility of HV test points in modern generators and from the HV ripple. Since this ripple can vary from a few times power line frequencies to over 100 kHz, broad band frequency compensated dividers are required whose calibration is not easily assured [4]. These difficulties have prompted development and application of several noninvasive alternatives.

The principal noninvasive techniques in fairly widespread use at present include differential x-ray filter methods [5, 6, 7], which are particularly convenient for testing clinical installations, ionization spectrometry, which is more frequently applied in standardizing laboratories [8, 9], and Compton scattering spectrometry [10, 11, 12]. Although the latter two methods offer high accuracy (*ca.* 0.2 kV) and are readily calibrated with respect to radioactive sources or x-ray emission line standards, acquiring the needed spectral data during the interval of a standard clinical exposure is somewhat difficult owing to the time required for event-by-event photon counting. Procedures using differential filters offer greater simplicity, convenience, and are less expensive relative to the other two methods. Differential filter methods that use two thicknesses of the same element have a wider range of application but a more slowly varying response to HV changes [13, 14, 15, 16] as compared to methods using absorbers with a critical threshold in the range of interest. Both of these filtration methods, however, require some calibration since the response functions are sensitive to target material, intrinsic filtration and electrical waveform (High-performance differential filter kVp meters generally require separate calibration settings according to anode type, filtration, and,less frequently, high voltage waveform). A less widely used variant of the critical filter method, developed at the National Physical Laboratory (NPL) in the UK, is based on detection of fluorescent x-rays from the absorber [17].

In an effort to overcome the limitations of previously available methods, we have demonstrated the effectiveness of a particular form of wavelength-dispersive crystal diffraction spectrometry. This method has high intrinsic precision and accuracy; it is self-calibrating and capable of acquiring spectral data in parallel at arbitrarily high rates, permitting its application to clinical sources operated at full power. This new technology obviates the need for invasive electrical measurements, overcomes the limitations inherent in filtration and fluorescence threshold methods, and has produced results whose accuracy exceeds clinical requirements.

Aside from its accuracy and its adaptability to the clinical setting, the NIST spectrometric procedure gives not only the high energy limit of the continuous x-ray spectrum (which is numerically equal

to the voltage applied to the x-ray source) but also the entire spectral profile, including the effects of both inherent and added filtration. This capability invites potentially more discerning studies of the variation of image quality as a function of deliberately introduced changes in the overall spectral distribution. A further use of this overall spectral information is to detect target deterioration due to the transport of filament material (tungsten) and of the cathode support structure (frequently nickel). Such processes occur naturally over the long term even with conservative operation of an x-ray source and much more rapidly with less careful operation. It is at least plausible that such spectral degradation should effect diagnostic efficiency.

Background of previous work. To demonstrate the practicality of this approach, we first built a small spectrograph using symmetric Laue diffraction according to a format introduced early in this century by Rutherford and Andrade [18]. The original prototype spectrometer and experimental arrangement is illustrated in Figure 1(a). It shows a small focal spot x-ray source, a diffraction crystal (originally employing the silicon [220] reflection in a flat crystal geometry), an intermediate aperture and an image registration plane, illustrated as x-ray sensitive film. Although the absolute lattice parameter of the crystal is accurately known in terms of the fundamental standards, it is not a necessary input for energy calibration since emission and/or absorption features in the spectra are otherwise known with an accuracy of the order of 10 ppm or better. Such information provides an internal calibration for the pattern of images seen on a film or other imaging detector.

An example of a densitometer trace for a film exposed in the device illustrated in Figure 1(a) is shown in Figure 1(b). Note that each spectral feature is duplicated, once on a leftward oriented dispersion curve and once rightward. This mirror-symmetric duplication eliminates the troublesome question of where the recorded spectrum begins. Figure 1(c), shows an expanded view of the region near the end-point energy. The intersection between the indicated background and the linearly varying continuum distribution, which gives the accelerating potential applied to the x-ray source, is clearly discernable with an imprecision of 0.1 kV, a level of refinement that exceeds the needs of mammographic practice as they are currently understood. Should further refinement be needed, it is straightforward to achieve 10 V accuracy by modifications of the apparatus.

In more recent work we have addressed important limitations of the flat crystal x-ray optics illustrated in Figure 1(a), namely its dependence on focal spot size and low sensitivity. Specifically, resolution (and hence voltage precision) depends on the x-ray focal spot size which, though adequate in newer sources, is highly variable among older installations. To circumvent this limitation, we have begun to make use of the focussing crystal optics illustrated in Figure 2. This geometrical change has several consequences among which are: enhanced spectral dispersion so that a curved Si [111] crystal provides dispersion equal to that of the Si [220] flat crystal which had proven adequate, the larger structure factor for Si [111], and finally significantly increased efficiency of the spectrometer due to the focussing action of the curved crystal.

Purpose of the Present Work.
The overarching purpose of the work supported by this grant was to contribute to mammographic quality control by developing a self-calibrating spectrometer which provides accurate, non-invasive measurement of kV and the spectral output of an x-ray source. The three main goals which guided the work were:

(1) To move from film to solid state image registration:
A more desirable modality for use in the field was use of electronic imaging technology interfaced to a portable computer. The main direction of this work was toward use of available phosphors,

CCD's and image acquisition and analysis software.

(2) To increase the detection quantum efficiency (DQE) of the device:
The narrow diffraction widths (~ 1-2 eV) of perfect crystals used in the original prototype imply a considerable loss in x-ray sensitivity relative to a more optimally matched window with a width of about 100 eV. As one remedy, we tried by various means to introduce a deliberate gradient in the crystal's interplanar spacing whose effect was to increase the acceptance bandwidth and hence the instrument's efficiency. In search of larger integrated reflectivity than the Si systems used in previous work, we also systematically studied a cohort of crystals which had appropriate lattice spacings and could be bent elastically. Modifications of the sensor electronics and phosphor conversion layer were also investigated to enhance the DQE.

(3) To perform clinical studies:
Our goal, in collaboration with various groups, was to demonstrate the applicability and ease of use (including portability) of this new device in a clinical setting to calibrate the high energy applied to mammographic x-ray sources. In the process we expected to observe challenges which would lead to refinements of the spectrometer design. We also sought to take advantage of the full spectral characterization available since it allows study of new target and filter combinations, anode contamination, and, from existing clinical installations of varying ages, operating modalities and histories.

Methods of approach.
Crystal preparation, theoretical modeling, spectrometer manufacture, evaluation of imagers, image reduction and analysis, and the development and testing of advanced prototypical systems were conducted within the Physics Laboratory of NIST using our workshop and laboratory x-ray sources.

The range of needed clinical studies and the qualified personnel required were outside the scope of the technical development program at NIST. Accordingly, on the basis of initial expressions of interest by several clinically based groups, a letter was circulated suggesting the formation of a loose coalition of such investigations, all of which would be given access to prototype instrumentation from the NIST program. The first partnership was established with the Center for Devices and Radiological Health (CDRH) in the FDA's Rockville laboratories (Twinbrook Building 1). The initial clinical collaborations included: Georgetown University Medical Center, the University of Alabama Medical Center, and the University of California, Davis. The device was also exercised at Fisher Imaging, Radcal Corporation, Schick Technologies, and the NIST mammographic calibration facility. The general idea was to facilitate rapid, parallel investigation along the main coordinates in the parameter space associated with physical source characteristics.

Experimental Methods and Results of Present Work

This grant has supported a number of critical developmental improvements of the spectrometer/detection system, calibration procedure and formalism, as well as initial testing in a variety of clinical settings. The primary methods and results of this work are organized below in seven sections:

(I) Utilization of an inexpensive scheme of digital registration of spectral images.
(II) Optimization of overall system performance including crystal and sensor modifications.
(III) Mounting of the spectrometer in a positioning device; packaging a compact and portable system.
(IV) Performance Estimates.
(V) Initial studies in a clinical setting.
(VI) Extensions to higher and lower energies
(VII) Derivation of an analytic curved crystal dispersion function in Cauchois geometry.

(I) Utilization of an inexpensive scheme of digital registration of spectral images.

Photographic registration of spectral data, as used in our earliest flat and curved crystal prototype spectrometers, entailed an inconvenient delay for film development and densitometry, and the background noise was a limiting factor. One of the main goals of this work was to find suitable electronic imaging technology which is also interfaced to a portable computer to facilitate immediate analysis in the field. While almost all forms of direct electronic x-ray imaging are, in principle, applicable to the current problem of spectral registration, the need for a simple, low cost system with adequate sensitivity led fairly rapidly to a focus on optical charge coupled devices (CCD's) with phosphor conversion layers. We considered both the use of fiber optic tapers with minification to small (low cost) CCD's and direct (1:1) use larger format imagers.

Our current systems take advantage of recently introduced large area digital radiography sensors which are now being used in place of dental film. Because of the logarithmic response of photographic film, these CCD-based sensors do not possess comparable dynamic range but they do possess greater sensitivity and contrast. In the present work we use a size 2 dental sensor from Schick Technologies, Inc.[19] It has an active area of 36.5 x 25.2 mm and 760 x 524 square pixels 48μm on a side. It is packaged in an anodized aluminum case as a 6 mm thick sandwich consisting of a scintillator, fiber optic faceplate, CCD and I/O cable. The sensor is supported by a drive electronics module and power supply which is connected in turn to a PC-based 8-bit ISA bus interface card. Software is provided that can capture 12-bit images for a user-specified amount of time at a spatial resolution of 9-10 lp/mm. This type of a system is rendered economical by of the use of a biasing scheme which greatly suppresses the collection of dark current providing high signal to noise at room temperature without the requirement of active cooling.

A schematic of our most recent prototype is shown in Figure 2. A two-dimensional color image acquired with this spectrometer and digital sensor is shown in the top portion of Figure 3. A background (dark) image has been subtracted to remove fixed-pattern noise. The spectrometer used a Si(111) crystal of 185μm thickness bent to a radius of six inches. In the center, one sees the structure of the focal spot of the x-ray source imaged by a pin-hole camera which is on the center axis of the spectrometer. The pinhole is in the center of the faceplate and estimated to be about 10 μm diameter. The column-summed profile of this image is shown in bottom of Figure 3. This projection is the one-dimensional spectrum which is used in practice to extract the energy applied to the x-ray source or study the spectral distribution.

(II) Optimization of overall system performance including crystal and sensor modifications.

In September 1994 an early S[111] prototype spectrometer was taken to the Twinbrook Building 1 laboratories, Rockville, MD of the FDA's Center for Devices and Radiological Health (CDRH) for a field trial with a mammographic x-ray source. Results were promising until a 30μm Mo filter was inserted into the incident x-ray beam. The effect of the loss in signal due to absorption in the filter raised concern over the increase in uncertainty over the position of the high-energy cutoff. This becomes increasingly important at lower energies because the generally reduced x-ray source power and output. Since many field mammographic sources contain permanently mounted filtration, we were motivated to undertake further development to increase the sensitivity of the device, even at the cost of some loss of spatial resolution.

Dental x-ray sources are intense relative to our application and generally operated at around 70 keV. To increase the sensitivity of the CCD detector system, we first increased the system gain by a factor of five by replacing a resistor in the drive electronics module. In this configuration one sees a modest thermal background grow in during the few seconds of a typical measurement using one of our low-current laboratory x-ray sources. This modest "fogging" as well as artifacts due to point defects in the CCD are largely offset by image subtraction of a dark image acquired with the same time as the exposed image.

A second step toward gaining higher sensitivity, albeit at some cost in resolution, involved substituting a high sensitivity phosphor screen for the normal, thinner directly applied phosphor converter. The higher sensitivity x-ray intensifying screen used was a 150 μm-thick convertor of doped Gd_2O_2S. The sensitivity increase obtained through this change was a factor of $4 \pm 5\%$ over the energy range used in mammography. This substitution had the unwelcome but tolerable effect of reducing the spatial resolution of the sensor from 9 to 10 line pairs per millimeter (lp/mm) to about 6 lp/mm.

A third obvious place to gain spectral throughput is in the choice of diffracting crystal. The range of crystals and diffraction planes which might be used in the present application is constrained by several technical considerations. Among these constraints, the size range of economically acceptable imagers and the working distance limitation to the focal spot are the most obvious. Besides Si[111] we tested several other crystal planes which had lattice spacings appropriate to this application [Ge(111), PET(020), LiF(200), Qz(10-1-1)] which could both be cut so as to provide a high-reflectivity plane in transmission and also bent elastically to a small radius of curvature without breaking. The alternative crystals examined and their relative performance parameters are summarized in Appendix A. The current crystal of choice is natural quartz (Qz) with the $(10\bar{1}\bar{1})$ planes active. This material is readily available and plates sufficiently thick (about 0.25 mm) for efficient diffraction are elastically bendable to the needed radius (15 cm). In comparison with the results obtained initially from Si (111) (thickness 0.185 mm), the transmitted intensity is larger by a factor of about eight due primarily to the elastic (quasimosaic) Sumbaev effect [20] in quartz as discussed in Appendix A. In combination with the modified detector, the system sensitivity is more than a factor of thirty greater than our initial curved-crystal prototype (not counting the increase in the electronic gain). As a consequence, spectra from filtered sources can now be easily registered within the exposure time of a normal mammographic exposure. This is true for the unmodified, higher-resolution CCD sensor except under conditions of low kV and heavy filtration.

These gains in sensitivity positioned us to resume field testing of the spectrometer system in the

final phase of this work. We were able to acquire suitable spectra from filtrated sources within the time of a standard clinical mammographic exposure. Indeed, the data in Figure 4 were taken using our most advanced prototype under the "worst case" conditions of low HV (22 kV), heavy filtration (25 μm of molybdenum), and only 85 mAs of exposure. The inset graph shows the region of the endpoint energy and the scale of 1 kV in this energy region (thirteen pixels).

(III) Mounting of the spectrometer in a positioning device; packaging a compact and portable system.

Efforts have also been directed toward realizing more convenient packaging, enhanced portability, and ease of installation and use. The present system consists of a low-cost notebook computer with a single, internal ISA bus which holds the CCD interface card. This fits conveniently in a normal size briefcase with the interface power supply, calibration foils, and some small tools. The spectrometer itself is mounted with three degrees of freedom as illustrated schematically in Figure 5. After it is placed on a standard mammographic platform, its height is adjusted with a vertical translation stage to the nominal working distance of 20 cm from the focal spot. The kV results are relatively insensitive to this parameter and the needed accuracy of a few centimeters is obtained with a measuring tape. Gross spectrometer positioning is aided by viewing the shadow pattern of the entrance baffle on the sensor package using the field illumination lamp available in most mammographic systems. This image is visible because of the transparency of both the quartz analyzing crystal and the lead acrylic top of the spectrometer body. Final alignment is done with x-rays. We have performed initial testing of this prototype spectrometer with a variety of clinical sources. Set up and alignment generally took about ten minutes. On occasion, adequate alignment was more elusive. In such cases, time could be saved with the use of interchangeable pinholes of various sizes and a retractable crossover slit. Fine lateral tuning is accomplished by a screw-driven adjustment in the plane of dispersion to center the image of the focal spot between the two mirror-image x-ray spectra. This is done iteratively by adjusting the position between test exposures until centering is achieved to within a few tenths of a millimeter. There is also an alignment bubble on the base of the spectrometer holder. Finally, the spectrometer's supporting cradle allows its plane of dispersion to be tilted with respect to the vertical so as to accommodate different anode orientations. When either a different anode track or filament is used, some fine repositioning may be needed to re-center the image on the sensor.

(IV) Performance Estimates

Preliminary results have been obtained using several laboratory x-ray sources with Mo anodes[1)] and at several clinical sites. The data discussed in this section were obtained using a quartz crystal spectrometer with modified sensor head and sensor electronics. A group of spectra illustrative of what would be obtained in a clinical calibration sequence is shown in Figure 6. These spectra are from a source with no intrinsic filtration, however the spectra are modified by addition of a 1 mm Al filter to reduce the range of intensities applied to the imaging detector. In practice, such spectra would more likely be obtained at intervals of 1 kV rather than at the 5 kV intervals indicated. These particular spectra were obtained in a laboratory environment with a small focus source and a low ripple HV supply and normalized to a common exposure; each was acquired with less than 60 mAs. The formalism developed in Appendix B has been applied to extract the end-point energy of

---

1) In house laboratory work used a compact microfocus source of a type available for magnification mammography (Tru-Focus MXT 7100 Moly x-ray tube with 0.15 mm focal spot) or a Ge-CA8L Mo tube with nominal focal spot of 1.3 mm.

spectra acquired in the laboratory and in the field; the results are discussed below. Installations having large amounts of HV ripple will give spectra whose end-point profiles are less sharply delineated. On the other hand, the associated spectra accurately portray the time-averaged radiation profile used.

Analysis of a series of spectra (such as that of Figure 6) is particularly simple when acquired with a flat crystal spectrometer [2]: the location of a single spectral feature pair is sufficient to calibrate the instrument to extract the voltage applied to the x-ray source. The formalism derived in Appendix B (equations 10 and 11) shows that, in contrast with the flat-crystal case, a curved crystal spectrometer has four independent parameters in a nonlinear dispersion function relating lateral image displacement from the center of the detector to energy: r, d, i, and s; a fifth parameter, detector pixel size, is needed to relate pixel number to actual displacement. To calibrate such a camera, one could, in principle, measure each of these geometrical parameters with attention to their respective sensitivities. (For example, an uncertainty in the radius of curvature of the crystal of 0.5 mm introduces an uncertainty of 0.1 keV in the end-point energy at a voltage of 32 kV.) Any or all of these geometrical measurements may be eliminated by using an equal number of spectral markers of known energy, including characteristic spectral lines from the anode and absorption edges. The edges can be easily superimposed on a spectrum by placing thin foils between the source and the spectrometer.

However, as further shown in Appendix B, curved-crystal-spectrometer calibration can be much simpler, indeed comparable to the case of the flat-crystal spectrometer. The exact, nonlinear dispersion relation connecting E to x can be replaced by a simpler, linear relation between E^2 and x^{-2},

$$E^2 = \frac{a}{x^2} + b,$$

to an accuracy of better than 1 eV over the range of energies and spectrometer configurations of interest to mammographic calibration. The two coefficients, a and b, of this linear approximation of the dispersion function can be determined from the geometrical parameters of the spectrometer, as derived in Appendix B, or, perhaps more practically, from a calibration involving at least two spectral features of known energy.

To obtain an initial estimate of the absolute accuracy that might be obtained using the technology described in this report, we first calibrated the detector scale of a spectrometer, in the approximation shown above, with the positions of the K-edge of thin foils of tin, cadmium, silver, and palladium. Operationally, "positions" are defined as half the distance between identical features of the left and right recorded spectra; this tends to reduce errors due to imperfect alignment of source, crystal, and detector in the plane of dispersion. The position of an edge was defined as the half-height of the natural logarithm of the inverse of the intensity. The residuals due to fitting the dispersion function to the foil edges were all less than 0.02 kV. We then used this calibration to determine the endpoint energies of a series of spectra (such as shown in Figure 6) recorded at six voltages between 22 kV and 36 kV. Endpoint positions were determined by fitting to the region of the endpoint to a function that is linear above the endpoint energy and cubic below the endpoint. We compared these extracted endpoint energies with concurrent measurements of a voltage divider connected to our laboratory x-ray source supply. The step-down resistor was itself calibrated at NIST in the Electrical Engineering Laboratory. Careful application of this methodology provided agreements to within 0.1 kV over the energy range used for mammography. The uncertainty in this scheme is dominated by uncertainties in the determination of the endpoint locations and in the calibration of the voltage divider rather than any intrinsic property of the spectrometer itself. We estimate that this level of accuracy could be significantly improved by more sophisticated modeling

of the high-energy endpoint region and edge transmission function and by higher resolution image registration. Table1 below compares the voltage as determined by the spectrometric method developed under this grant to that measured by the Electricity Division (Dr. Martin Misakian) of NIST over a broad range of energies.

Table 1: Comparison of Results of Spectrometric and Voltage Divider Methods of kV Determination

Spectrometer (V)	NIST Voltage Divider (V)	Difference (V)
20156	20123	33
30092	30004	88
34970	34977	-7
40043	40025	18
44474	44691	-217
50105	49980	125

(V) Initial Studies in a Clinical Setting.

At the invitation of Bob Jennings and Phil Quinn we obtained valuable experience using x-ray sources at the Twinbrook Building 1 laboratories of the Center for Devices and Radiological Health (CDRH/FDA). These visits gave us early indication of the demanding sensitivity that would be required to obtain images during a typical mammographic exposure with heavy filtration. Bob Jennings and Bob Gagne also asked us to work at NIH where we made measurements from a Eureka tube and a Mammomat 2 tube. The purpose of these visits was to help resolve an energy discrepancy between one of these sources and a source at the Rockville campus. We also were able to note by now that some of the clinical sources we tested possessed scattered radiation that could contribute a non-uniform background to the spectrum. This in turn can increase the uncertainty with which the endpoint energy can be extracted. It was found that a transverse pre-aperture either attached to the source side of the spectrometer or somehow otherwise inserted between the source and spectrometer could block this radiation which is scattered from the walls of the source and transmitted through aperture A of Figure 2 without being diffracted. The results of a study of the focal spots of the two FDA sources is shown in Figure 7. It was observed that the shape and position of the beam spot changed as a function of source current.

An early prototype spectrometer was sent to Dr. John Boone, Associate Professor of Radiology, UC Davis Medical Center, U. S. Army Breast Cancer Research Program grant #DAMD17-94-J-4424. Results were included in his mid-term report to the U. S. Army Breast Cancer Research Program. He also requested an instrument which would take spectra to lower energies. As described in section VI, we developed a prototype which easily measured spectral emissions down to 12 kV.

We were asked to energy-calibrate the x-ray sources at the NIST mammography calibration program (Bert Coursey and Michelle Johnson). In addition, registration of the spectral distribution permitted the identification of anode contamination. Figure 8 shows the presence of silver contamination while using a molybdenum anode and trace indium contamination in the spectrum from a rhodium anode.

The spectrometer described in this study has been patented and licensed to the Radcal corporation in Monrovia, CA. They are first marketing it as a research device and have already received orders and are producing the first production units. They plan to begin making deliveries before the end of calendar 1996. A field instrument for mammography will be developed next and targeted at the medical physics and compliance market. Beyond that, Radcal will develop a field instrument for general radiographic energies (40 - 150 kV). The field instruments will probably employ additional detection devices for radiation dose, exposure duration, and waveform.

Additionally, the spectrometer has been exercised at ISIS, Department of Radiology, Georgetown University (Hamid Jafroudi), Fisher Imaging (Michelle Picarro), and Schick Technologies (Dan Neugroschl). It is also being made available to Dr. Gary Barnes at the University Of Alabama Medical Center for extended studies.

(VI) Extensions to higher and lower energies.

By choice of lattice spacings and/or spectrometer dimensions, this spectrographic technique is also extensible to energy regimes both lower and higher than that employed in mammography. We first investigated the higher energy regime used in diagnostic radiography. To accommodate the smaller Bragg angles associated with these higher energies, we used an extended version of the spectrometer shown in Figure 2 which was configured for a source to crystal distance of 1120 mm and a crystal to image plane distance of 370 mm. High-energy spectra were obtained using the (220) diffracting planes of a germanium crystal bent to a radius of 370 mm and x-ray sensitive film. The tungsten anode source used had a 3.8 mm x 3.8 mm focal spot and 7 mm Be window; an attenuator of 0.25 mm of Mo was added to reduce the dynamic range of the spectra. In this preliminary work, no attempt was made to match the full spectral image pattern (width 45 mm) with the size of the available dental CCD (width = 37.5 mm) so that we registered only one of the two mirror-symmetric spectra as shown in Figure 9 for applied x-ray voltages in the range of 100 to 160 kV. The spectra show the W K-alpha (59 keV) and K-beta (67 keV) emissions and a high-energy cutoff of the continuum radiation with an acceptable ratio of signal to noise. Background images were subtracted before generating the pixel column sums. Each of the spectra was acquired with 10 mA source current and have been normalized to exposure time. The 100 kV spectrum was acquired with about 650 mAs; 120 kV, 350 mAs; 140 kV, 270 mAs; 160 kV, 230 mAs. These exposures can be reduced by optimizing the screen thickness for higher energies. Image quality in higher-energy radiological applications is less sensitive to applied source potential. These applications, however, do depend upon HV stability and reproducibility. This is because dosimeters used to standardize exposure employ gas ionization by x-rays which is a strongly varying function of incident photon energy.

At the request of one of our coalition partners, Dr. John Boone, Associate Professor of Radiology, UC Davis Medical Center, U. S. Army Breast Cancer Research Program grant #DAMD17-94-J-4424, we have built and delivered a working prototype spectrometer which registers spectra down to below 12 kV. It employs a more transparent CCD faceplate (0.5 mm of lucite), a relatively thin x-ray convertor, and the use of the $(10\bar{1}0)$ planes of quartz which have a lattice spacing of 0.426 nm. The quartz crystal was about 280 μm thick and bent to a radius of curvature of 145 cm to match the image width to that of the sensor. A spectrum from this low-energy device is shown in Figure 10. It is apparent that the system sensitivity has yet to be challenged even down at 12 kV.

Dr. Boone is using this spectrometer as a research tool but notes its potential as a quality-assurance tool, vastly simplifying the physicist's MQSA (Mammography Quality Standards Act) responsibilities at clinical mammography sites. He sites the following as an example:

"Much of the measurement protocol is designed at gathering indirect evidence of suitable x-ray beam characteristics, for example the half value layer (HVL) is a measure of how much aluminum is required to reduce the intensity of the x-ray beam by a factor of 1/2. The HVL is an indirect measure of the mammography machine's x-ray spectral performance. Typically the HVL measurement requires on the order of 3 to 5 x-ray exposures (at several kVs). The diffraction spectrometer, however, has the potential to give its user a much more complete, direct measure of the x-ray beam characteristics in just one exposure."

Dr. Boone is also seeking to calibrate not only the energy axis of the acquired spectra but also the intensity axis. Using absolute x-ray spectra measured by Mr. Tom Fewell at CDRH, intensity calibration curves as a function of energy were derived for diffraction spectrometer data. Correction of spectrometer data compared favorably with CDRH spectra acquired under similar conditions.

(VII) Derivation of an analytic curved crystal dispersion function in Cauchois geometry.

The dispersion function for a spectrographic instrument is the relation between the transverse coordinate in the spectrometer's image plane and the energy (or wavelength) of the x-rays registered at that position. While this function has a very simple form for the flat crystal geometry [2], the present curved-crystal geometry entails greater complexity [3]. The derivation which follows assumes ideal alignment of source, crystal, scatter baffle and plane of detection (effects of misalignment are discussed in reference [21]). As shown in Figure 11, the crystal has a radius of curvature r, the imaging detector is located a distance i away from the crystal and the source is located a distance s away from the crystal along a perpendicular to the detector. For this derivation, consider x-ray emission only in the plane of the figure; large out-of-plane diffraction would result in curved spectral "lines", but this is not evident in the images acquired with the spectrometers described here. The ray path indicated leaves the source and is diffracted by the crystal at a Bragg angle θ, and impinges on the detector plane at the distance x from the spectrometer centerline. Since symmetric Laue case diffraction is not encumbered by an index of refraction correction, the diffraction angle, θ, is simply related to x-ray wavelength, λ, and energy, E, through: $\lambda = \frac{2d}{n}\sin\theta$ and $E = \frac{hc}{\lambda}$ with hc = $1.9864475 \times 10^{-25}$ J·m (1.23984244 nm·keV) [22] where d is the lattice spacing of the crystal, n is the order of diffraction. n = 1 in the cases considered here.

The dispersion function derivation is simplified by introducing a new parameter, u, which is functionally related to the Bragg angle through $u = \sin\theta$. In terms of this new parameter, a series of geometrical relationships (given in Appendix B) can be arranged to give:

$$x(E) = [r + (i - r)v]\frac{u}{w}$$

where

$$v \equiv 2\sqrt{1-u^2}\sqrt{1-f^2u^2} - f(1-2u^2)$$
$$w \equiv (1-2u^2)\sqrt{1-f^2u^2} + 2fu^2\sqrt{1-u^2}$$
$$f \equiv r/(r+s)$$
$$u = E_0/E$$
$$E_0 \equiv nhc/2d.$$

In practice, one is interested in E(x), in which case the equation shown above can be numerically inverted. This inversion is easily addressed in the numerical algorithms which would be used for extracting spectral distributions and end-point energies. In the special case where $r = i$, it is then possible to express E(x) parametrically or as an unwieldy analytic expression. An example of this dispersion function is shown in Figure 12(a) for the spectrometer shown in Figure 11. Here the Si(111) planes are used in first order with d = 0.3136 nm, $r = i$ =150 mm and with the source placed s = 210 mm from the crystal. It is clear from Figure 12(a) that the number of pixels/kV decreases along the detector as one approaches, from either direction, the centerpoint of the two spectra—which itself is at zero wavelength or infinite energy. The simple behavior of the dispersion curve in Figure 12(a) invites use of empirical approximations over limited energy ranges. For example, the expression $E^2 = \frac{a}{x^2} + b$ can replace the exact, inverted dispersion relation E = E(x) with an imprecision of less than 1 eV over the range of energies used in mammography. (We are indebted to J.H. Marshall, Radcal Corporation, Monrovia, CA for pointing out this particular form for approximating the dispersion relation. This form is discussed further in Appendix B.) In Figure 12(b), the data of 12(a) are replotted as E^2 versus x^{-2} to suggest application of a linear approximation.

Conclusions

Three goals are outlined above in the Introduction under the heading Purpose of the Present Work. In their abbreviated form they are:

(1) To move from film to solid state image registration.
(2) To increase the system detector quantum efficiency.
(3) To perform clinical studies of performance and usability.

Due in no small part to the support provided by this grant, all of these goals have been met. A low cost imaging system was discovered and modified. In its optimized form it will initially be used in the commercial spectrometer produced by Radcal Corporation. Through selection of an optimum diffracting crystal plane and sensor modifications, the system sensitivity is now such that statistically-good images may be acquired within the parameter space of a normal mammographic exposure. Initial clinical studies provided feedback for refinements in spectrometer design as well as practical issues of packaging and usability. Using the spectrometer system, calibration procedure, and formalism described in this report, x-ray tube voltage may be determined to less than 0.1 kV over the mammographic energy regime. This exceeds the needs of mammographic practice as they are currently understood. Finally, we have demonstrated the capability of extending this method to higher and lower energy regimes.

Future potential: With regard to the registration of the spectral distribution, there are two main issues that could be further explored: (i) First it is conjectured that the full spectral characterization of test systems including conventional and novel x-ray sources with an extended range of filtration options will lead to either improved technique outside of the presently considered parameter space or to an appreciation that the present range of source and filter combinations is already optimal. (ii) Second, it is proposed that spectra produced in the cohort of x-ray tubes currently in clinical use may not be adequately represented by their nominal anode composition at the time of manufacture. If this spectral variability is, in fact, encountered, then it would be of considerable interest to determine the extent to which these changes influence diagnostic efficacy (at the level of phantom-based scoring procedures).

Figure Captions

Figure 1: (a) Diagram of an early flat-crystal prototype instrument for determining both end point energies and overall spectral distributions emitted by mammographic x-ray sources. (b) Typical densitometer tracing from a film exposed in the spectrometric apparatus of Fig. 1(a). The needed energy scale can be established either by length metrology or by referring to the well-established energy values for the characteristic x-ray lines or edges shown. (c) An expanded view of densitometric measurements near the end-point energy (numerically equal to the kilovoltage applied to the x-ray tube). Here, refinement is clearly of the order of 0.1 kV.

Figure 2: Schematic diagram of a curved crystal modification of the spectrometric device shown in Fig. 1. Diagram of a curved-crystal spectrometer for energy calibration and spectral characterization of mammographic x-ray sources. X-rays originate at source S, are diffracted by crystal C through aperture A and are imaged at plane P. The dimensions shown are appropriate for use with a Si(111) crystal bent to a 15 cm (6 inch) radius of curvature.

Figure 3: Top: False color image of a molybdenum x-ray tube acquired with the spectrometer shown in Figure 2 acquired with the dental CCD described in the text. A pinhole-camera image of the focal spot is visible in the center of the image. Bottom: The pixel column sum of the image shown above. This shows the molybdenum spectrum (the alpha lines are saturated) with high-energy cutoff and, in the center, the focal spot image.

Figure 4: Low intensity spectrum acquired at 22 kV, 25 μm Mo filtration, and 85 mAs exposure.

Figure 5: Schematic of spectrometer and positioning system with a clinical mammographic x-ray source.

Figure 6: Series of calibration spectra at different energies filtered with 1 mm of aluminum.

Figure 7: A study of focal spots from two clinical mammographic x-ray sources at NIH.

Figure 8: Examples of anode contamination at the NIST mammographic calibration facility; identification is possible due to the spectrometer's acquisition of the spectral profile on an energy calibrated axis. Similar contamination has been observed at other facilities.

Figure 9: High-energy spectra (100 to 160 keV) acquired with the dental CCD described in the text.

Figure 10: Spectrum from the low-energy prototype spectrometer described in the text. In this spectrum, the high-energy cutoff is 33 kV and the low-energy cut-off is 12 kV.

Figure 11: Schematic showing the geometry of the source, crystal, and detector used in derivation of the curved crystal spectrometer dispersion function. In particular, s is the distance from the source to crystal center, i is the distance from crystal center to detector, and r is the radius of curvature of the crystal.

Figure 12: Calculated dispersion function for the curved crystal spectrometer shown in Figure 2. (b) Data of Figure 12(a) replotted against a new set of variables.

Figure 13: The relative improvement in diffraction efficiency attained after an air-abrasive treatment of the surface of a Si crystal using the (111) planes in transmission.

Figure 14: Comparison of spectra acquired from an abraded Si(111) crystal (0.185 mm thickness) and a Qz $(10\,\bar{1}\,\bar{1})$ crystal (0.25 mm thickness).

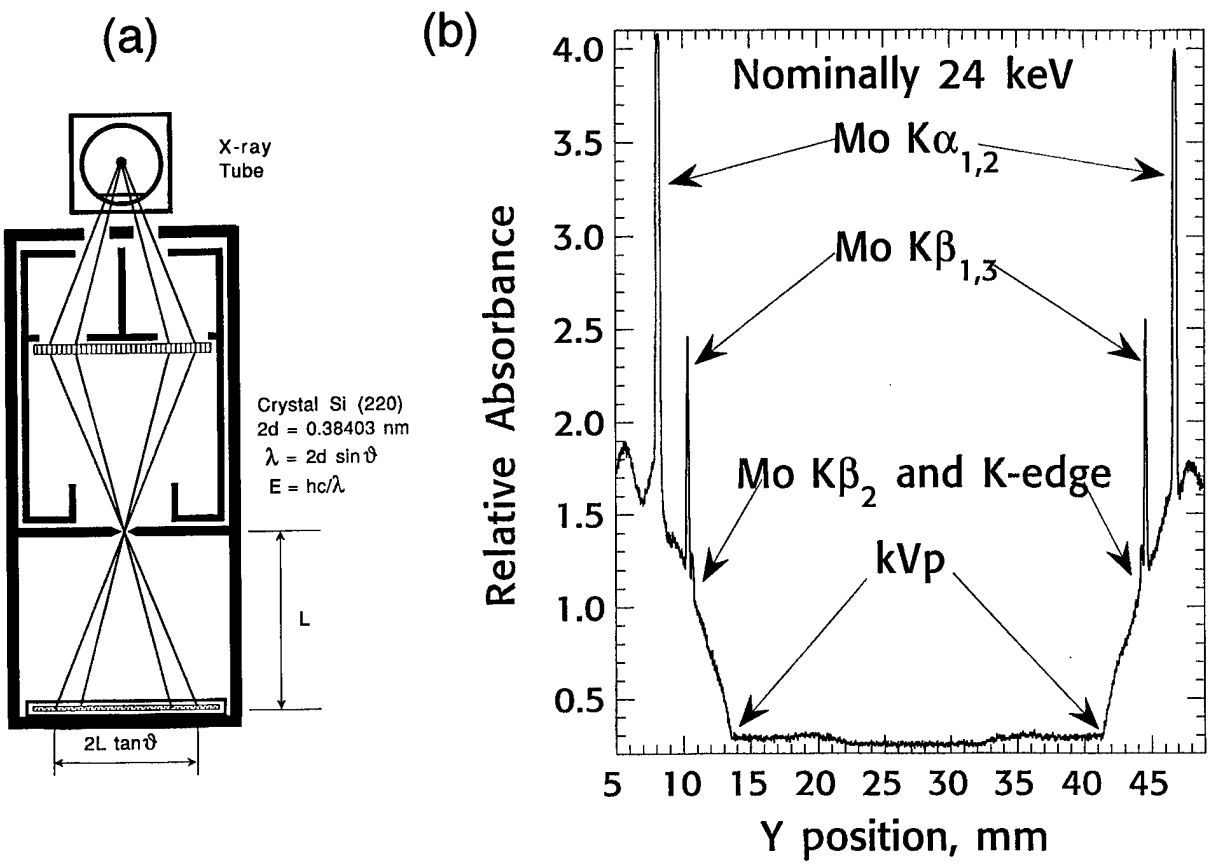
(a)
X-ray
Tube
Crystal Si (220)
2d = 0.38403 nm
λ = 2d sinϑ
E = hc/λ
L
2L tanϑ
(b)
Nominally 24 keV
Mo Kα1,2
Mo Kβ1,3
Mo Kβ2 and K-edge
kVp
Relative Absorbance
Y position, mm
(c)
24 kVp nominal
Relative Absorbance
keV

Figure 1

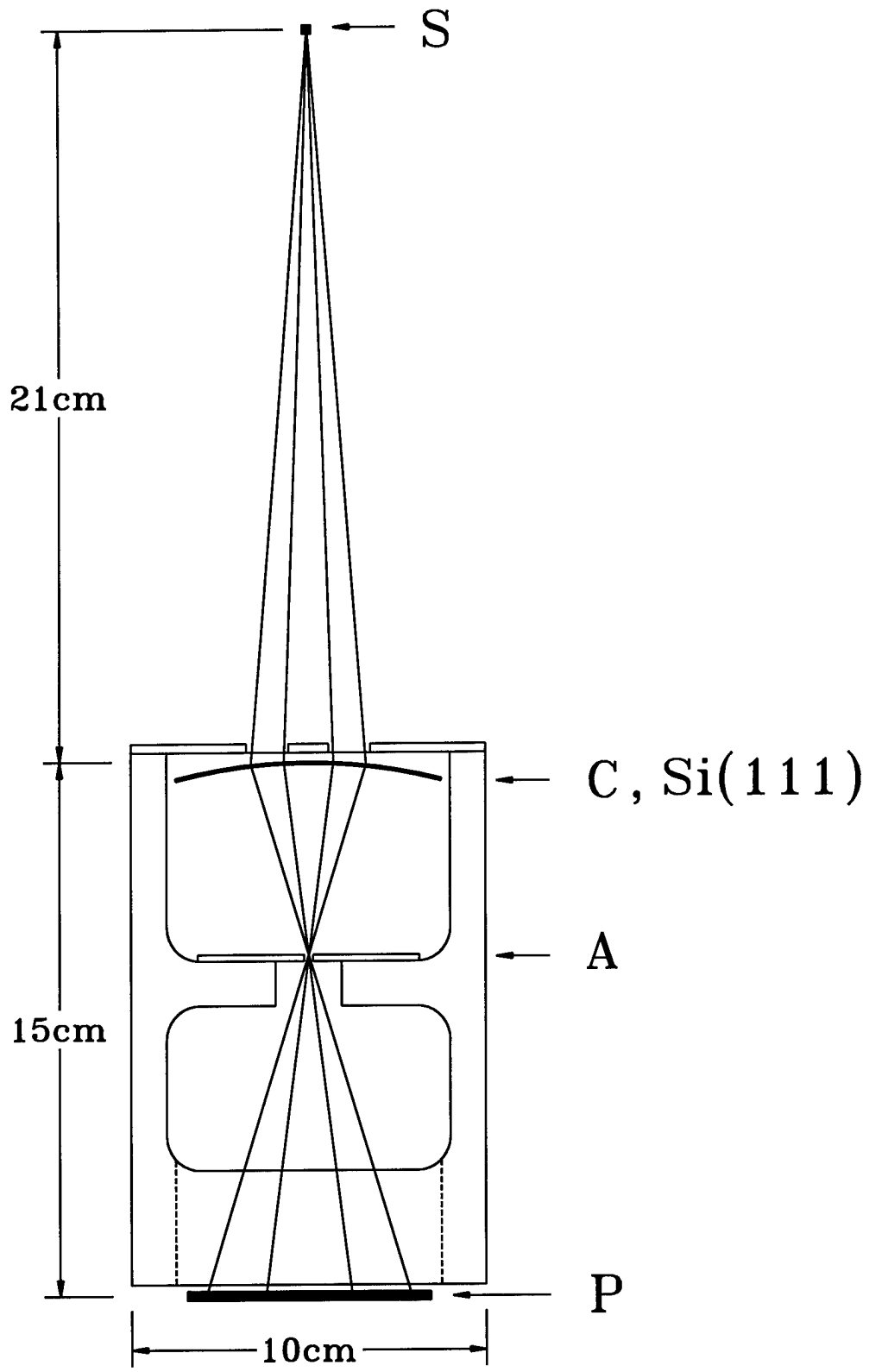

Figure 2

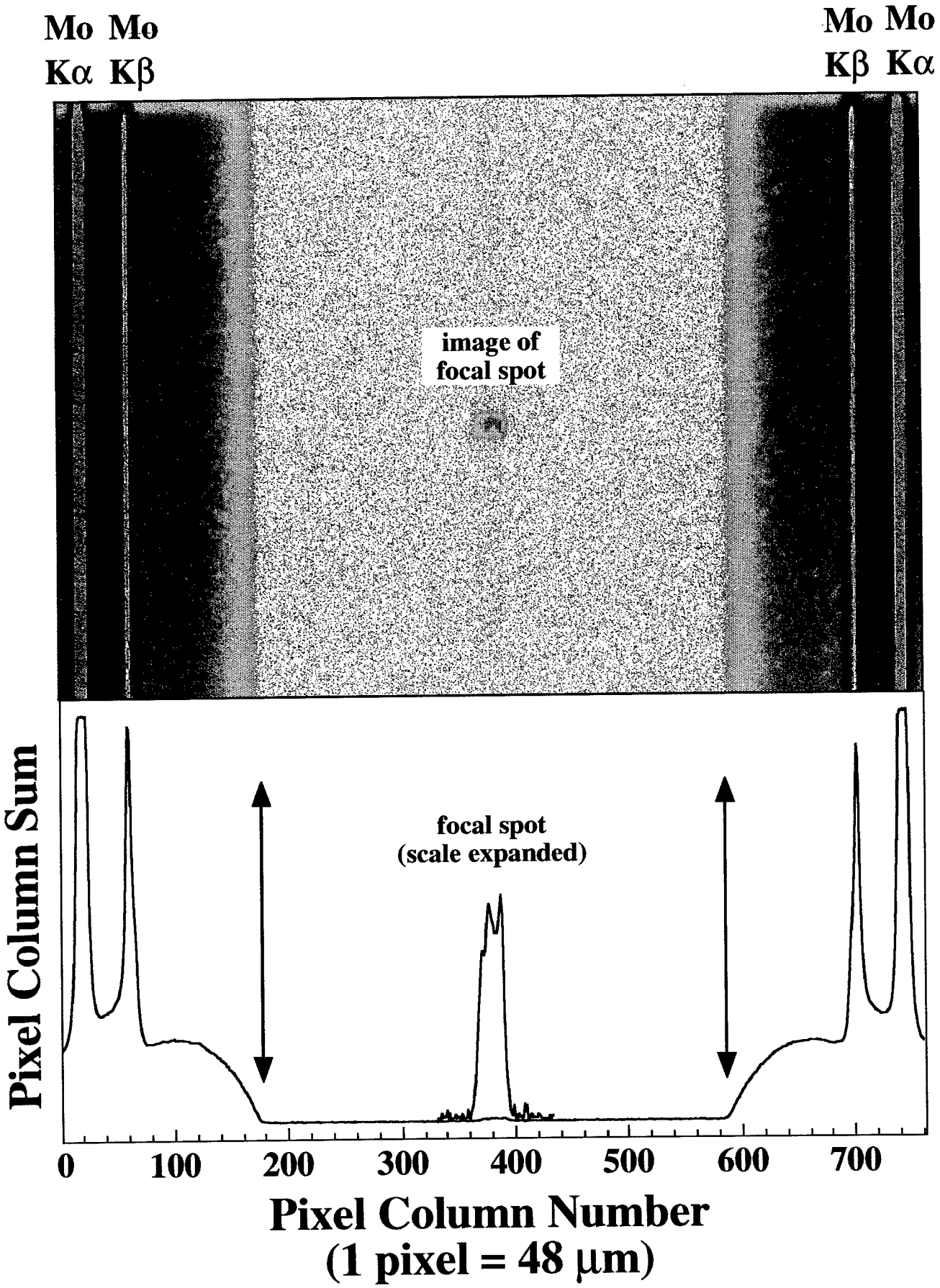
Mo Mo
Kα Kβ
Mo Mo
Kβ Kα
image of
focal spot
focal spot
(scale expanded)
Pixel Column Sum
0
100
200
300
400
500
600
700
Pixel Column Number
(1 pixel = 48 μm)

Figure 3

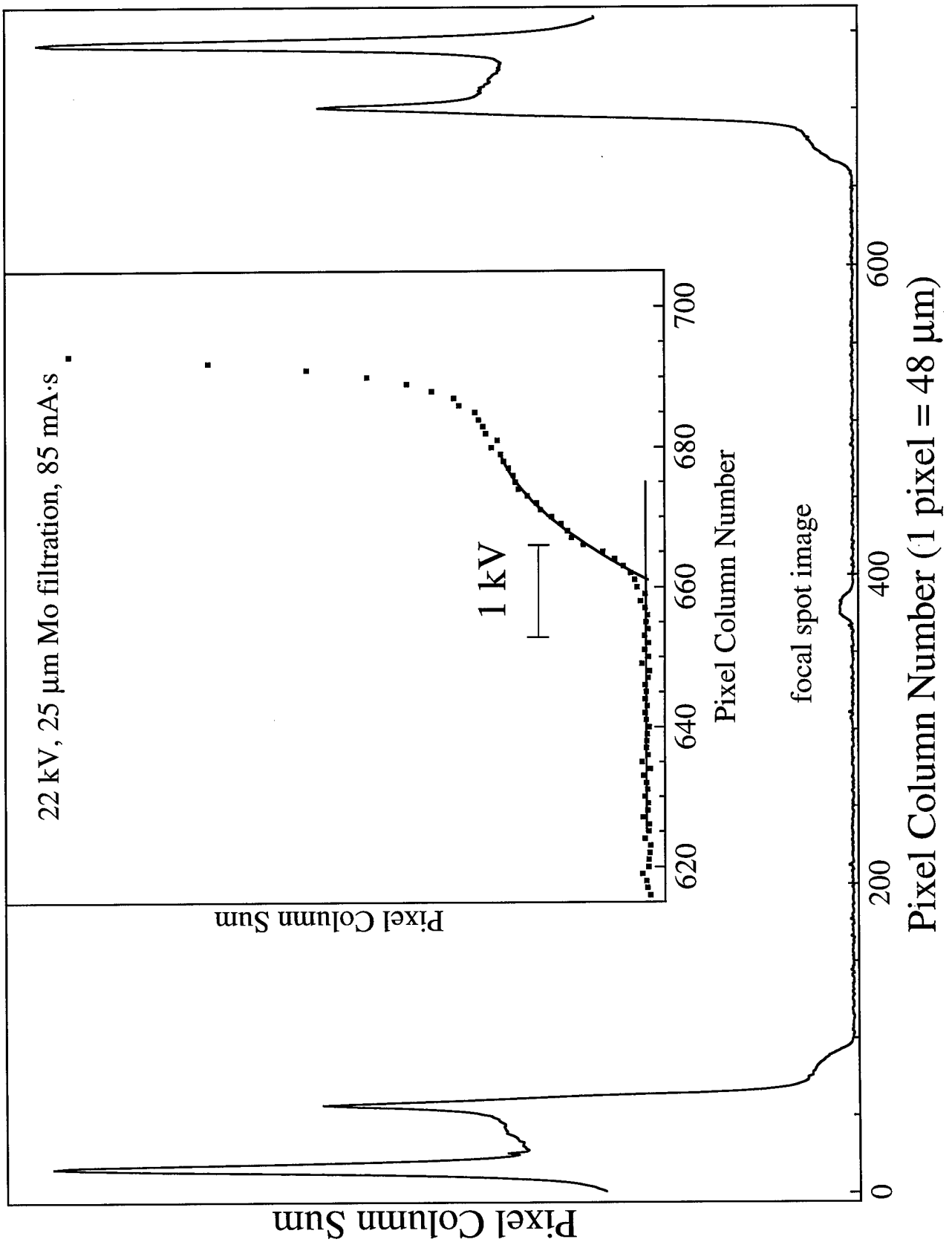
Pixel Column Sum
0
200
400
600
Pixel Column Number (1 pixel = 48 μm)
focal spot image
Pixel Column Number
620
640
660
680
700
1 kV
22 kV, 25 μm Mo filtration, 85 mA·s
Pixel Column Sum

Figure 4

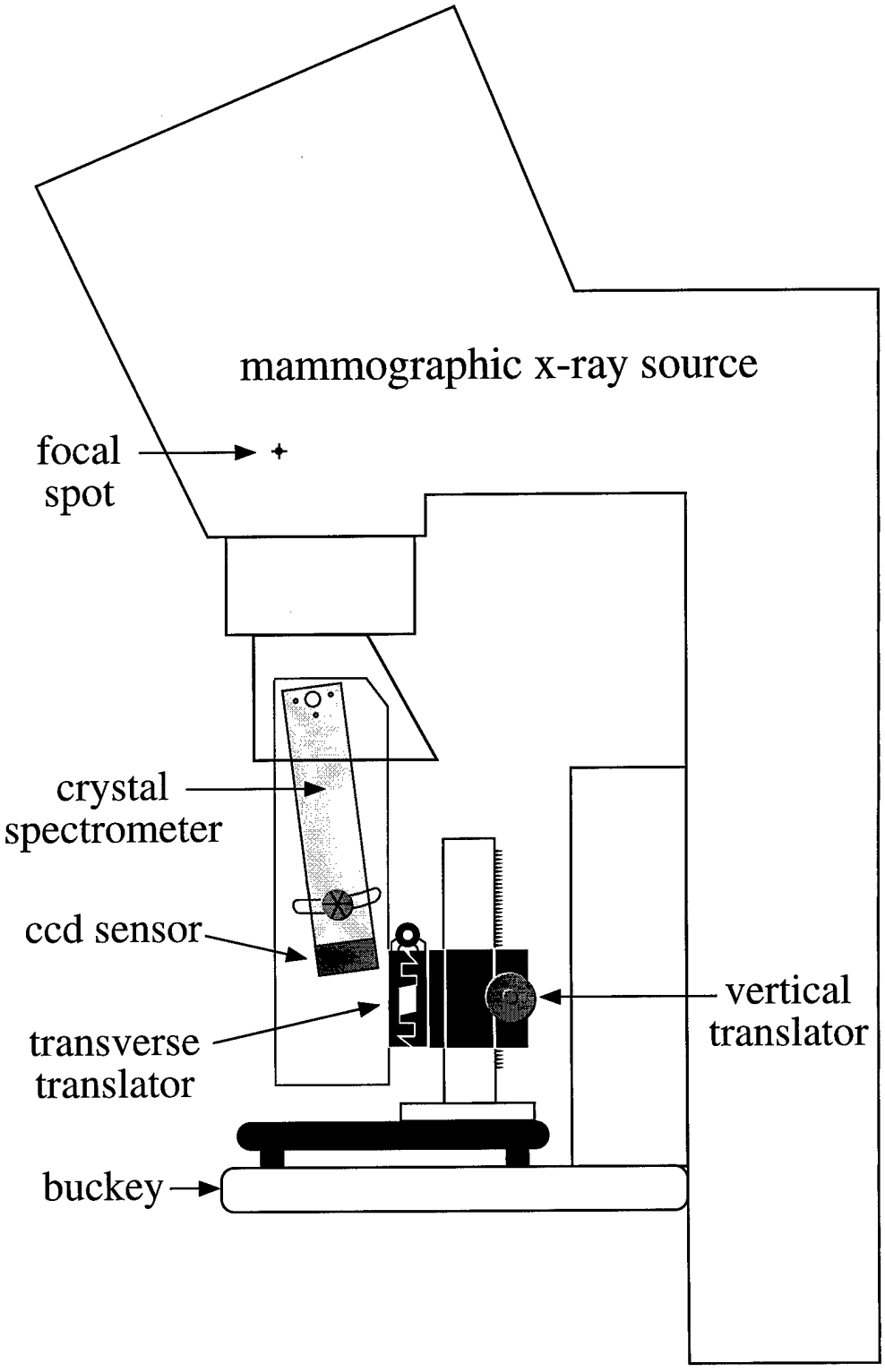
mammographic x-ray source
focal spot
crystal spectrometer
ccd sensor
transverse translator
vertical translator
buckey

Figure 5

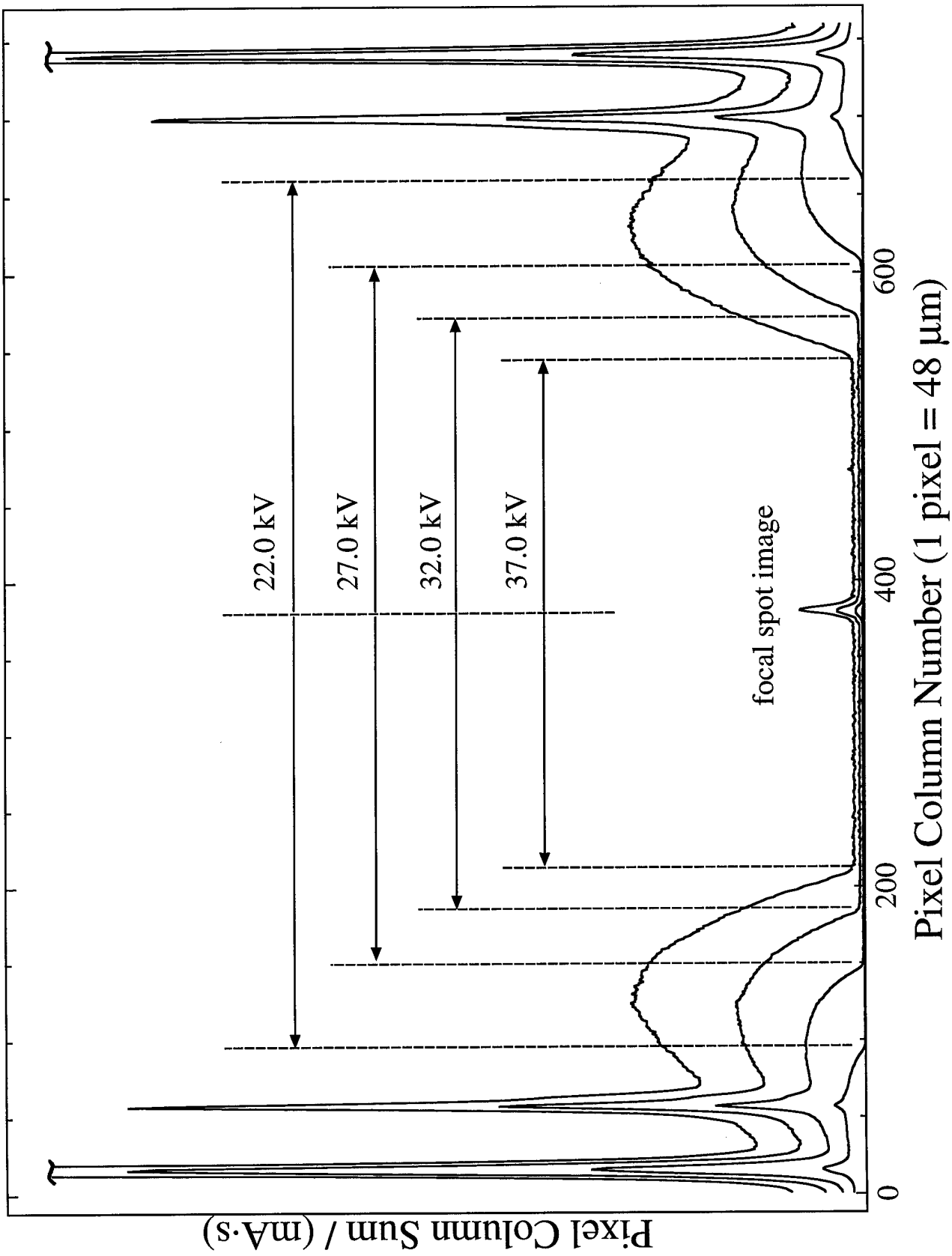
Pixel Column Sum / (mA·s)
Pixel Column Number (1 pixel = 48 μm)
0
200
400
600
22.0 kV
27.0 kV
32.0 kV
37.0 kV
focal spot image

Figure 6

A Study of Focal Spots at NIH

Eureka Tube

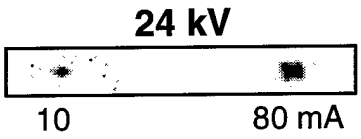

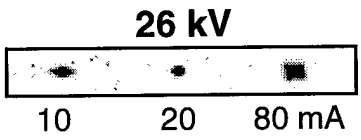

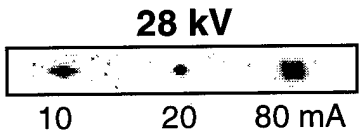

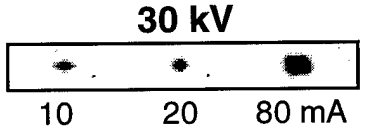

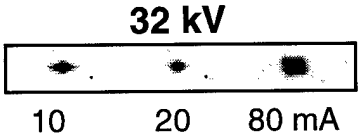

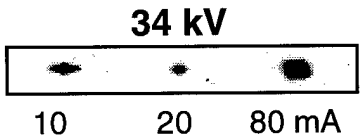

Mammomat 2

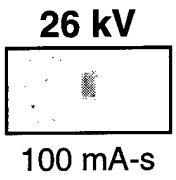

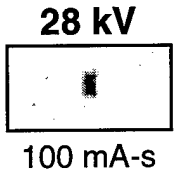

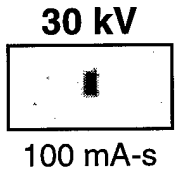

Images from the Eureka tube at 80 mA are about 8 x 8 pixels. For 20 mA, the diameter of the focal spot image is about 3.5 pixels. The dimensions of the Mammomat focal spot is about 5 x 9 pixels. A CCD pixel is 0.048 mm x 0.048 mm. The pinhole camera produced a minified image with the factor ~ 6 1/8" ÷ 9 1/2" = 0.645 for the Eureka source and a factor of 0.742 for the Mammomat source. Assuming that the finite extent of the pinhole added about one pixel of broadening in each dimension, then the approximate dimensions of the focal spots are:

Eureka 80 mA: 0.5 mm x 0.5 mm
Eureka 20 mA: 0.19 mm
Mammomat: 0.26 mm x 0.5 mm

When the Eureka source was changed from a small to a large focal spot, the centroid of the image of the focal spot moved about 20 pixels on the CCD. This corresponds to about 1.5 mm at the anode.

Internal structure is visible in the 80 mA images from the Eureka tube at lower energies. At higher energies, the sensor was run to saturation.

Figure 7

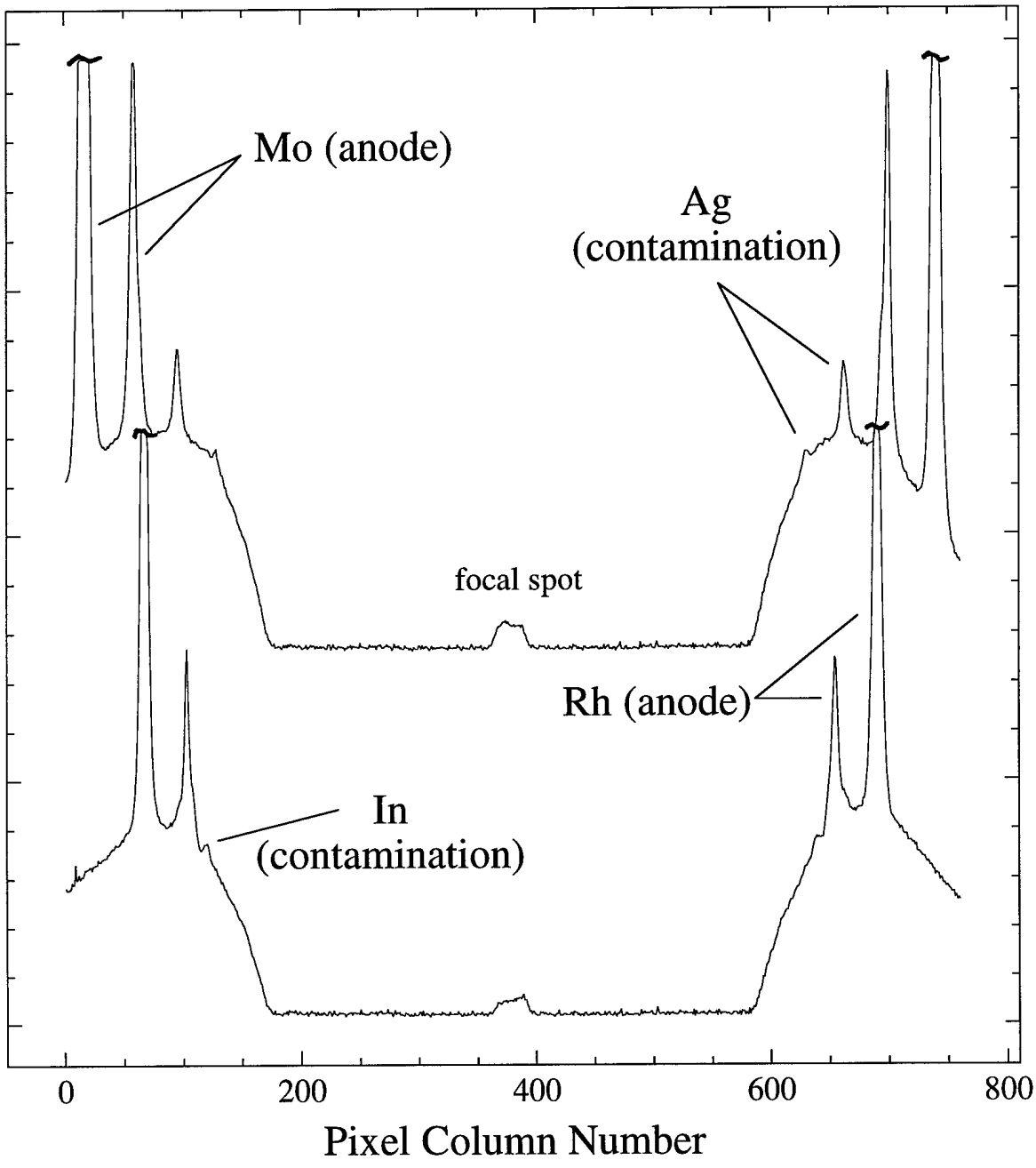
Mo (anode)
Ag
(contamination)
focal spot
Rh (anode)
In
(contamination)
0
200
400
600
800
Pixel Column Number

Figure 8

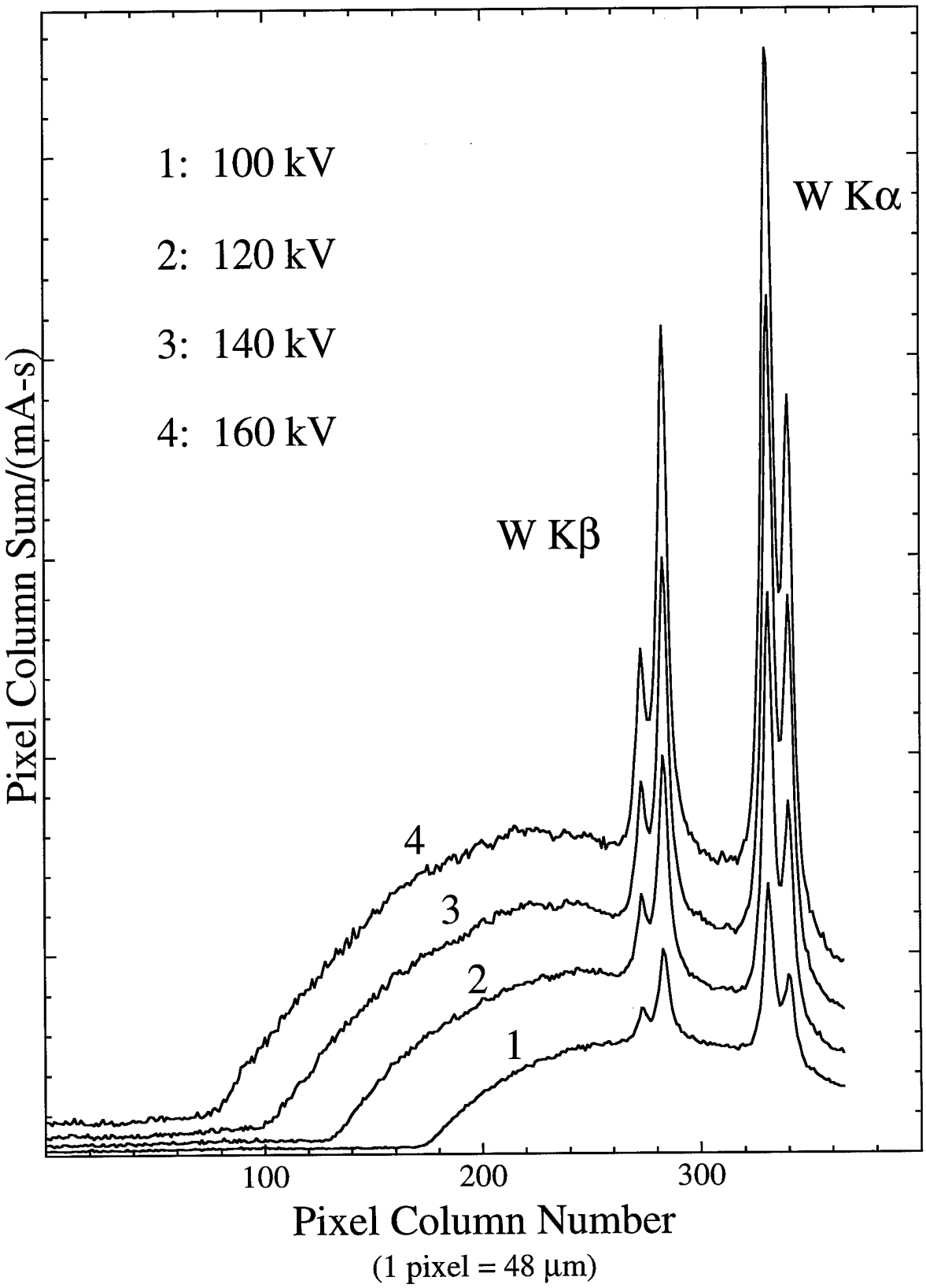
1: 100 kV
2: 120 kV
3: 140 kV
4: 160 kV
W Kα
W Kβ
4
3
2
1
Pixel Column Sum/(mA-s)
100
200
300
Pixel Column Number
(1 pixel = 48 μm)

Figure 9

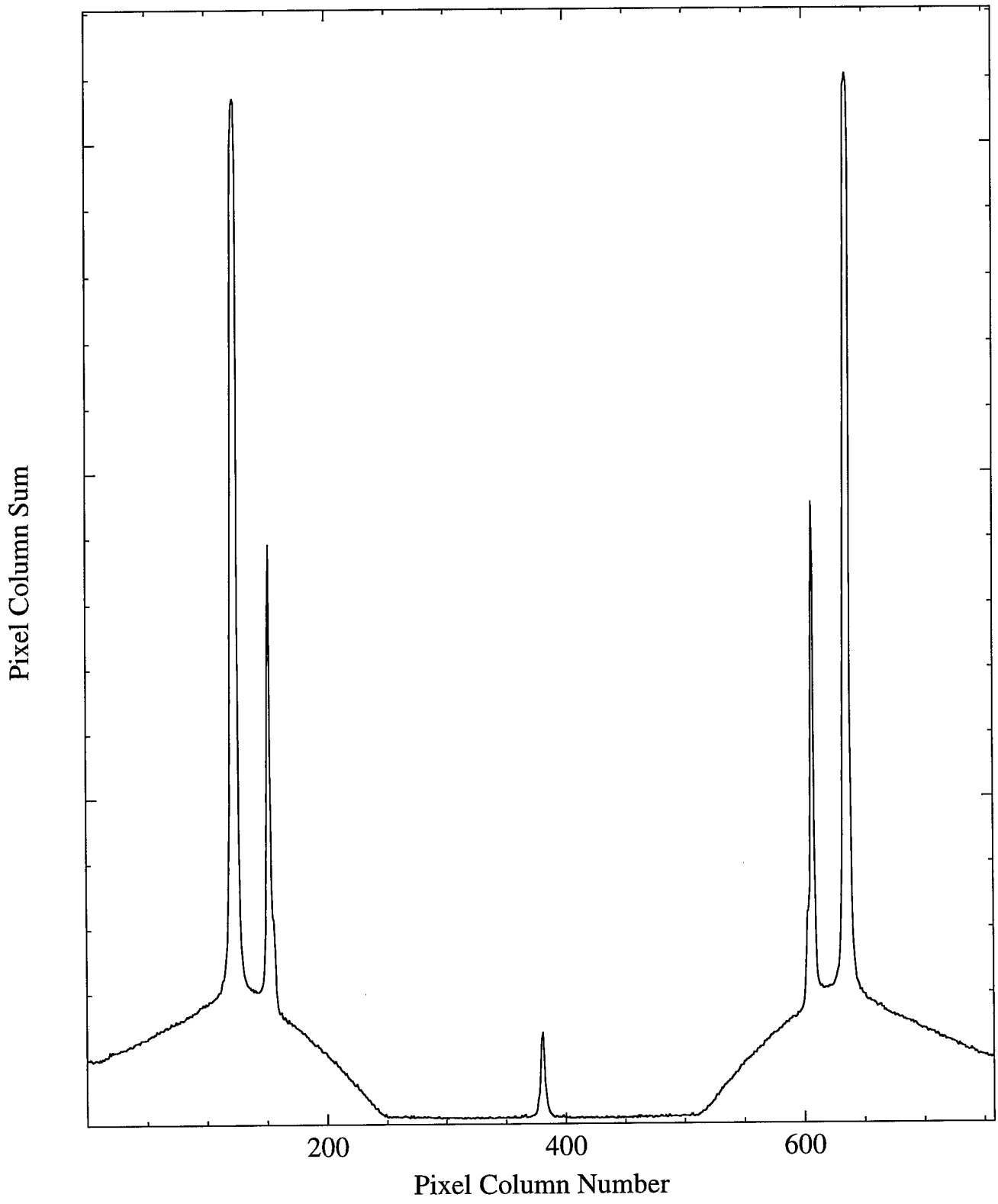

Figure 10

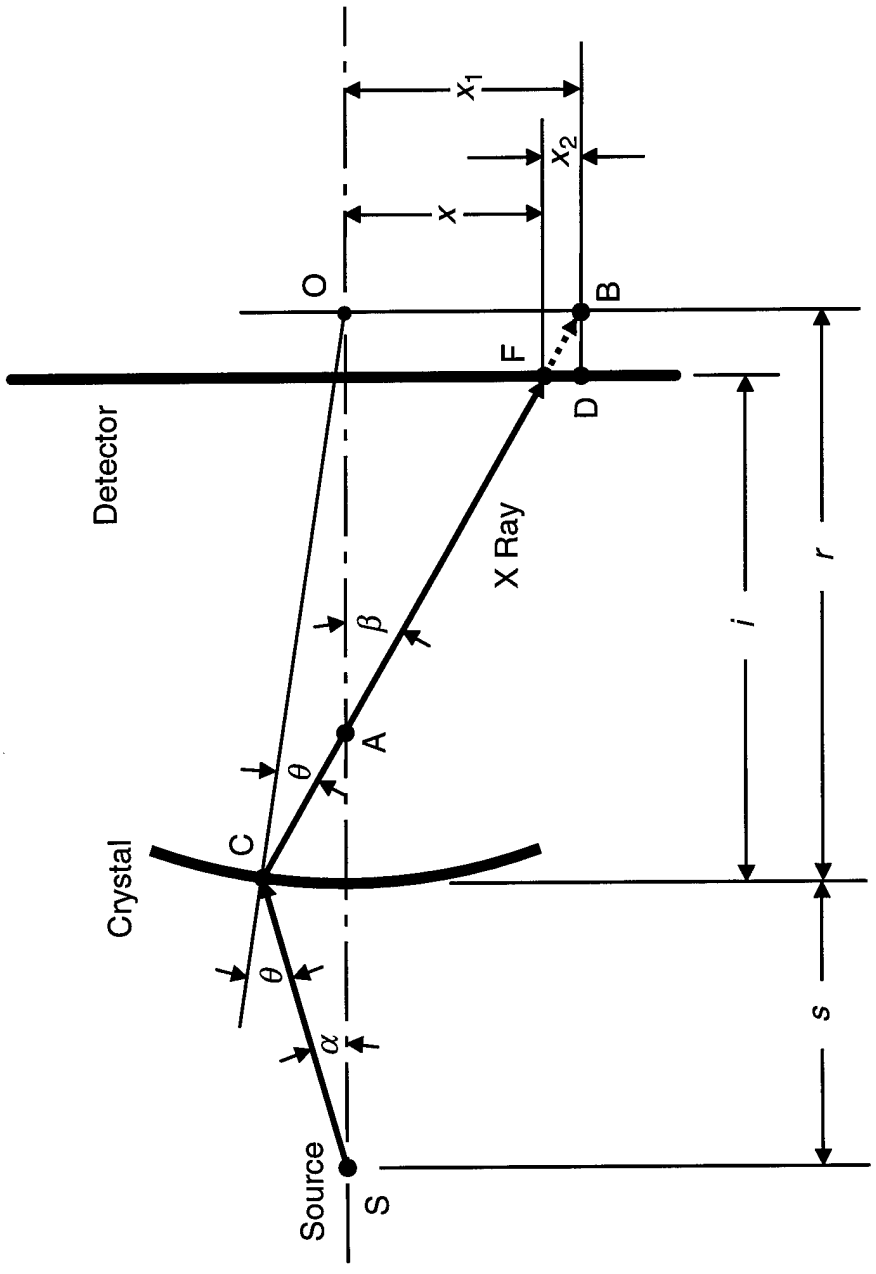
x_1
x_2
x
O
B
F
D
Detector
X Ray
β
i
r
A
θ
C
Crystal
θ
α
s
Source
S

Figure 11

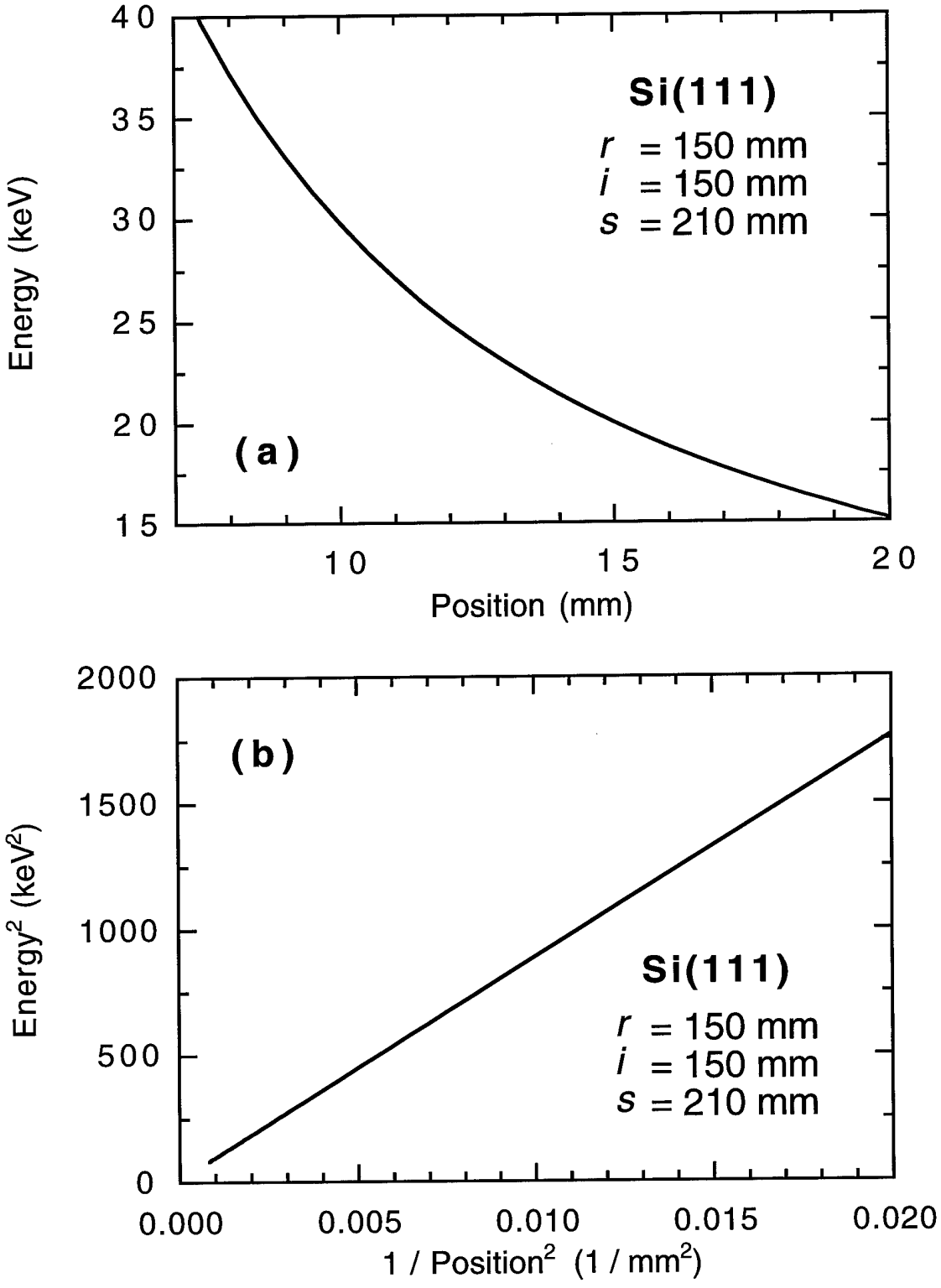
40
35
30
25
20
15
Energy (keV)
Si(111)
r = 150 mm
i = 150 mm
s = 210 mm
(a)
10
15
20
Position (mm)
2000
1500
1000
500
0
Energy² (keV²)
(b)
Si(111)
r = 150 mm
i = 150 mm
s = 210 mm
0.000
0.005
0.010
0.015
0.020
1 / Position² (1 / mm²)

Figure 12

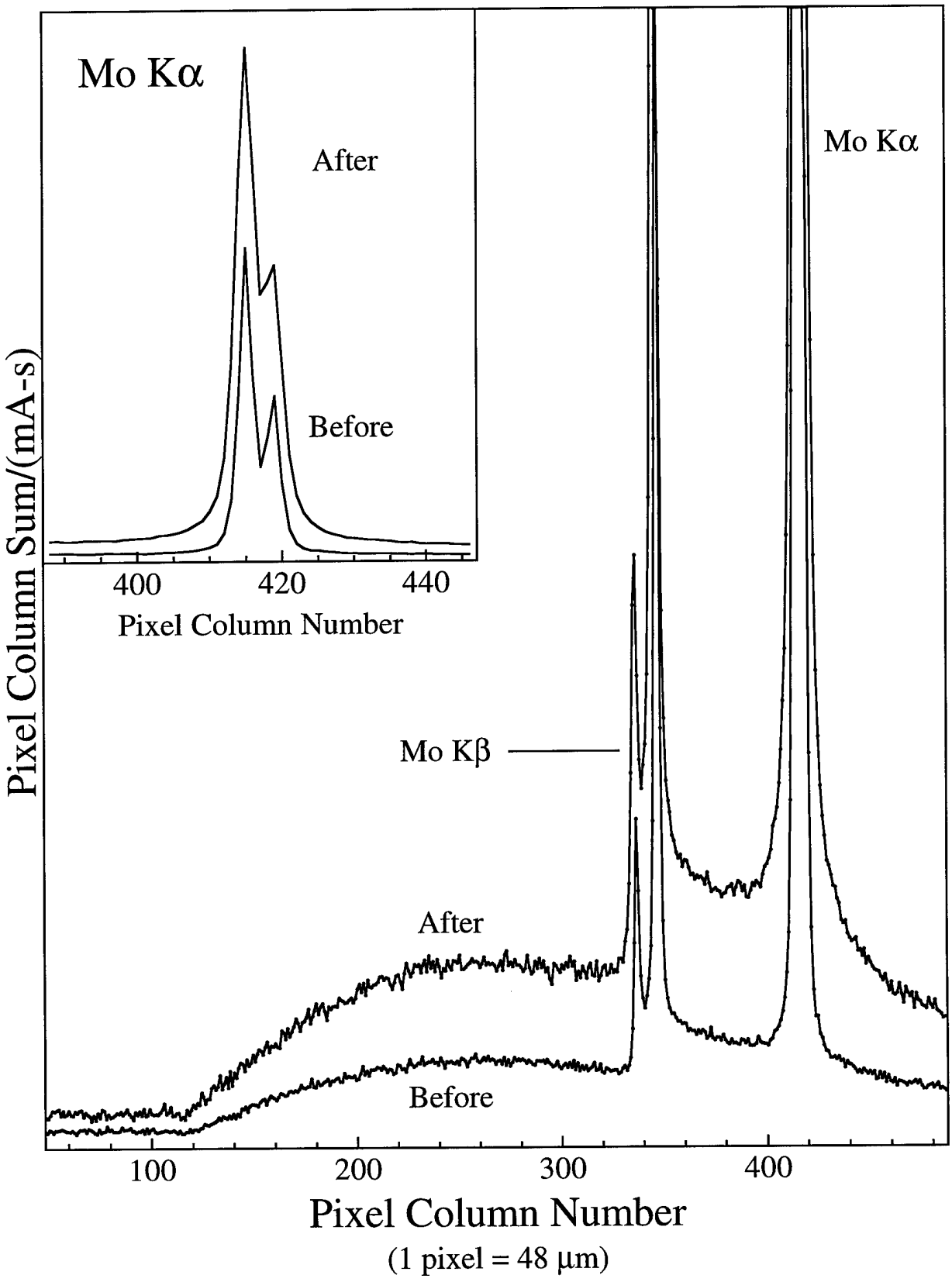
Mo Kα
After
Before
400
420
440
Pixel Column Number
Mo Kα
Mo Kβ
After
Before
Pixel Column Sum/(mA-s)
100
200
300
400
Pixel Column Number
(1 pixel = 48 μm)

Figure 13

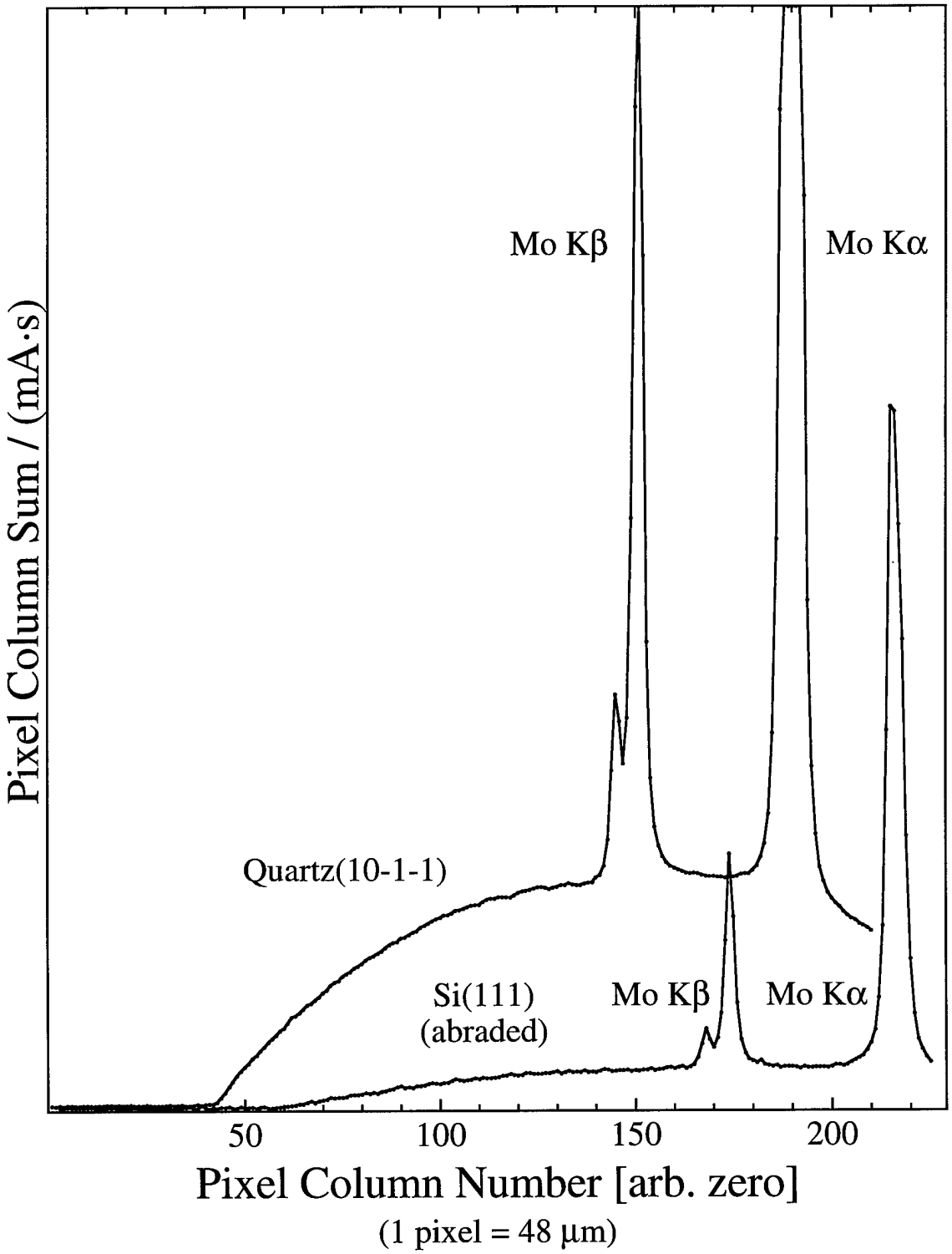
Mo Kβ
Mo Kα
Quartz(10-1-1)
Si(111)
(abraded)
Mo Kβ
Mo Kα
Pixel Column Sum / (mA·s)
50
100
150
200
Pixel Column Number [arb. zero]
(1 pixel = 48 μm)

Figure 14

References

[1] J. Law, K. Faulkner and S. Smith, "Variation of image quality with x-ray tube potential in mammography," Br. J. Radiol. **62**, 192-194 (1989); J. Law, "The measurement and routine checking of mammography x-ray tube kV," Phys. Med. Biol. **36**, 1133-1139 (1991).

[2] R. D. Deslattes, J. C. Levin, M. D. Walker, and A. Henins, "Noninvasive high voltage measurement in mammography by crystal diffraction spectrometry," Medical Physics **21** (1), 123-6 (1994).

[3] L. T. Hudson, R. D. Deslattes, A. Henins, C. T. Chantler, E. G. Kessler, and John E. Schweppe, "A curved crystal spectrometer for energy calibration and spectral characterization of mammographic x-ray sources," Medical Physics **23,** 1659-1670 (1996).

[4] Martin Misakian, "High Voltage Divider and Resistor Calibration," NBS Technical Note 1215 (July 1985), available from Superintendent of Documents, U.S. Government Printing Office, Washington, DC 20402.

[5] G. Hein, P. Pychlau, and E. Schüle, "NOMEX-A universal diagnostic dosemeter, mA·s, and kV meter for acceptance test measurements and quality assurance," Rad. Protect. Dosimetry **43**, 187-191 (1992).

[6] W. E. Simon and D. Richards, "Determination of x-ray tube potential (kV) wave form by a noninvasive evaluation of radiation output (NERO)," SPIE **273**, 149-152 (1981)

[7] W. E. Simon, "Noninvasive evaluation of a diagnostic x-ray machine using the Victoreen Model 6000A NERO," Br. J. Rad. Suppl. **18**, 96-99 (1985).

[8] J. R. Greening, "The measurement by ionizing methods of the peak kilovoltage across x-ray tubes," Br. J. Appl. Phys. **6**, 73-78 (1955)

[9] T. R. Fewell and K. E. Weaver, "The measurement of diagnostic x-ray spectra with a high purity germanium spectrometer," SPIE **56**, 9-18 (1975).

[10] G. Matscheko and R. Ribberfors, "A Compton scattering spectrometer for determining x-ray photon energy spectra," Phys. Med. Biol. **32**, 577-594 (1987)

[11] G. Matscheko and R. Ribberfors, "A generalised algorithm for spectral reconstruction in Compton spectroscopy with corrections for coherent scattering," Phys. Med. Biol. **34**, 835-841 (1989)

[12] G. A. Carlsson, K. Berggren, C. A. Carlsson, G. Matscheko and R. Ribberfors, "The Compton Spectrometer," Intl. J. Quant. Chem. **35**, 721-734 (1989).

[13] L. Stanton, D. A. Lightfoot, and S. Mann, "A penetrameter method for field kV calibration of diagnostic x-ray machines," Radiology **87**, 87-98 (1966)

[14] G. M. Ardran and H. E. Crooks, "Checking diagnostic x-ray beam quality," Br. J. Radiol. **41**, 193-198 (1968)

[15] A. F. Jacobson, J. R. Cameron, M. P. Siedband, and J. Wagner, "Test cassette for measuring peak tube potential of diagnostic x-ray machines", Med. Phys. **3**, 19-25 (1976).

[16] T. E. Sheridan, "Apparatus for measuring the peak voltage applied to a radiation source," US Patent No. 4843619, June 27, 1989, assigned to Kiethley Instruments, Inc.

[17] M. Davison and J. Law, "Measurement of the voltage of diagnostic x-ray tubes using K-characteristic fluorescence," Phys. Med. Biol. **17**, 572-576 (1972).

[18] E. Rutherford and E. N. da C. Andrade, "The spectrum of the penetrating x- rays from Radium B and Radium C," Phil. Mag. **28**, 263-273 (1914); ibid., "The wavelength of the soft x-rays from Radium B," **17**, 854-868.

[19] This does not constitute an endorsement by the United States Government but is given as a matter of information.

[20] O. I. Sumbaev, "Experimental investigation of the elastic quasi-mosaic effect," Soviet Physics JETP **27**, 724-728 (1968).

[21] C. T. Chantler, R. D. Deslattes, A. Henins, and L. T. Hudson, "Flat and curved crystal spectrography for mammographic x-ray sources," Br. J. Radiol. **69**, 636-649 (1996).

[22] E.R. Cohen and B.N. Taylor, "The 1986 Adjustment of the Fundamental Physical Constants," CODATA Bulletin **63**, Pergamon, Elmsford, NY, 1-32 (1986).

[23] J. R. Schneider, O. D. Conçalves, A. J. Rollason, U. Bonse, J. Lauer, and W. Zulehner, "Annealed Czochralski grown silicon crystals: a new material for the monochromatisation of synchrotron radiation and x-rays above 60 keV," Nucl. Instr. and Meth. **B29**, 661-674 (1988).

[24] S. Brennan and P. L. Cowan, "A suite of programs for calculating x-ray absorption, reflection, and diffraction performance for a variety of materials at arbitrary wavelengths," Rev. Sci. Instrum. **63**, 850-853 (1992).

[25] In particular, the magnitude of the enhanced reflectivity of the (10-1-1) planes of curved quartz crystals in a transmission geometry is in agreement with that predicted by the dynamical diffraction calculations of J. H. Marshall, Radcal Corporation, Monrovia, CA, private communication.

Appendix A: Crystal tests of relative integrated reflectivities

The sensitivity of the curved crystal spectrometer is challenged by the common use of molybdenum filtration, the occasional use of an attenuator (used sometimes to compress the dynamic range of the incoming spectrum when the brightest features occur at the lower energies), and the reduced flux from x-ray sources at lower applied voltages. As discussed in the main text , this was partly offset by increasing the gain of the adc's of the image capture electronics and retrofitting the sensor with a higher sensitivity phosphor converter. In attempting to gain additional improvement in overall system sensitivity, we tested several diffraction crystals whose structure provided high reflectivity in transmission and whose mechanical properties permitted elastic bending to the required small radius without causing fracture. Our benchmark curved crystal was Si(111) with a thickness of 185 μm. Among the additional crystals investigated were Ge(111), LiF(200), abraded Si(111), heat-treated oxygen-doped Si, and Qz $(10\,\bar{1}\,1)$. The radius of bending is determined primarily by the atomic lattice spacing of the crystal and the requirement that the image be focused onto the face of the chosen detector. In this work we used a size 2 dental CCD with an active area of 36.5 mm x 25.2 mm.

It was natural to try a germanium crystal since, in flat plates, Ge provides higher integrated reflectivities than Si over the wavelength range of present interest. However, because of the lower tensile strength of Ge (in comparison with Si), the Ge had to be thinner (no thicker than 140 μm) in order to bend to a 15 cm radius of curvature without breaking. At this reduced thickness, we found Ge(111) to be less efficient in Laue (transmission) diffraction than Si(111) at 185 μm thickness. This difference was about a factor of two at 28 kV with greater disparity at lower energies. In this case, the higher absorption of Ge overcomes its higher reflectivity.

LiF(200) produced significantly brighter images than Si(111). For example, a 0.5 mm thick LiF(002) reflected about seven times more 28 keV light than a 185 μm thick Si(111). Unfortunately, the crystalline quality of commercially available LiF is poor and spectral lines are smeared. X-ray topography revealed multiple domains in our fusion-grown LiF crystal. The lattice spacing of LiF(200) would also require a heat-treatment to bend LiF to the 10.2 cm radius of curvature required to focus the image onto the presently used dental sensor without fracturing the crystal.

The narrow diffraction widths (~ 1 to 2 eV) of perfect crystals imply a considerable loss in x-ray sensitivity relative to a more optimally matched width (~ 100 eV) required in the present application. We tried, therefore, by various means to introduce a gradient in the crystal's interplanar spacing to increase the acceptance bandwidth and hence the instrument's efficiency. First we attempted to introduce a strain gradient near the surface of a silicon crystal by rouge polishing. This proved ineffective. In marked contrast, the application of an air abrasive treatment using fine aluminum oxide grit produced an energy-dependent increase of throughput—about a factor of two at 28 keV. This enhancement was quickly brought to saturation after a frosted appearance was produced on the surface; the effect was easily reproduced on other Si crystals. Spectra from before and after this surface abrasion treatment are shown in Figure 13. The lower two spectra show the enhancement of Bremsstrahlung intensity between Mo Kβ (19.6 keV) and the end-point energy of 33 kV. The inset spectra show the enhancement of intensity at Mo Kα (17.5 keV) and the concomitant loss of resolution. These data were acquired with a CCD dental sensor that had not been retrofitted with a thicker scintillating screen and hence still exhibit resolved Kβ emissions of Mo.

We also tested analyzing crystals of Si(111) which possessed defects distributed throughout the bulk [23] and so might be expected to exhibit even further enhanced throughput. These samples were cut from silicon which had been grown by the Czochralski technique and so contained an incorporated oxygen concentration of about 10^{18} atoms·cm^{-3}. The bulk defects are created by annealing at temperatures above 550°C which causes oxygen to precipitate as a form of silica. After annealing, great enhancements in the integrated reflectivity have been observed at 317 keV [23]. The integrated reflectivity at the lower energies used in the present application, however, is less sensitive to the creation of a relatively small mosaic spread; the results were comparable to that of untreated silicon at the resolution of the dental CCD.

Our present prototype spectrometers use quartz (SiO_2) analyzing crystals. The brightest peak in the quartz x-ray powder pattern is designated 101. Contributing to this peak are two differently oriented sets of diffraction planes with the same atomic spacing of 0.3343 nm. Calculations from the code of Brennan and Cowan [24] predicted that the $(10\,\bar{1}\,\bar{1})$ or so-called minor planes (also known as the z planes of quartz) would exhibit about a 50% higher reflectivity than the $(10\,\bar{1}\,1)$ major planes (also known as the r planes) at Mo Kα. Our supplier (Valpey-Fisher Corporation, Hopkinton, MA) provided polished crystals of natural Brazilian quartz cut to the dimensions 47.0 mm x 27.5 mm x 0.23 mm. The Qz $(10\,\bar{1}\,\bar{1})$ diffraction planes gave the highest reflectivity among the crystals tested. The spectra from Qz $(10\,\bar{1}\,\bar{1})$ and abraded Si(111) which are compared in Figure 14 were acquired under identical experimental conditions: 30 kV applied to a small focus Mo x-ray tube without added filtration for an exposure of about 20 mAs. Both crystals were bent to a radius of curvature of 15 cm. Since the reflecting planes used in the two crystals have slightly different atomic spacings, the energy scale of the two spectra is different; they have been offset along the abscissa axis to show the region near the end-point energies. A dark image has been subtracted in both cases before computing the column sum; the spectra are plotted on the same ordinate scale without offset. The Mo Kα emission saturates the CCD in the spectrum from quartz.

The data reveal that the diffraction efficiency from the quartz crystal used is about a factor of four to five greater than that from the abraded silicon crystal. Since the gain due to abrading the silicon crystal was up to a factor of two (Figure 13), there is a net enhancement of about a factor of eight between the two materials oriented as described. We measured the transmission rocking curves of these two materials in the form of flat plates at these given thicknesses and found their reflectivity at Cu Kα to be comparable. This result is in accord with the calculations of dynamical diffraction theory [24]. One contributing factor to the higher intensity in the spectrum recorded using bent quartz over that of bent silicon is that the tensile strength of quartz considerably exceeds that of Si, permitting the use of thicker crystals; in this case the quartz crystal is 250 μm thick while the silicon is 185 μm thick. But the primary cause is due to the so-called Sumbaev effect [20], which is known to be particularly pronounced in quartz. The enhancement arises from the behavior of the planes normal to the surface as the crystal is cylindrically bent. These reflecting planes elastically take the form of parabolic surfaces, producing a quasimosaic effect which significantly broadens the rocking curve; additionally it causes slightly different relative reflectivities for the two 'mirror' spectra registered. Cut for transmission, bent Si(111) does not exhibit the Sumbaev effect; our quartz crystals were cut with a tip angle such that this effect is near maximum. These aspects of x-ray diffraction in quartz emerge quite naturally from a more general treatment of x-ray diffraction in such structurally and elastically anisotropic crystals.[25]

Appendix B: Derivation of the curved-crystal spectral dispersion function and a linear approximation function

In this appendix, we give a derivation of the dispersion function for a spectrometer using the modified Cauchois geometry. We assume ideal alignment of source, crystal, scatter baffle, and plane of detection. As shown in Figure 11, the crystal has a radius of curvature r, the imaging detector is located a distance i away from the crystal and the source is located a distance s away from the crystal along a perpendicular to the detector. Consider x-ray emission only in the plane of the figure, *i.e.* assume the crystal has zero height. Let α be the emission angle of the x-ray from the source with respect to the perpendicular from the detector. The Bragg angle, θ, at which the x-ray is diffracted by the crystal is also indicated. X-rays impinge on the detector plane at an angle β as shown in the figure. The distance from the center of the detector to the point of detection of the x-ray is:

$$x = x_1 - x_2. \tag{1}$$

Consideration of the triangle BDF in Figure 11 shows that

$$x_2 = (r - i)\tan\beta. \tag{2}$$

Applying the law of sines to the triangle COB with the angles θ and $(\pi/2 - \beta)$ opposite the sides x_1 and r, respectively, leads to

$$x_1 = r\frac{\sin\theta}{\cos\beta}. \tag{3}$$

Inserting Equations (2) and (3) into (1) and rearranging gives

$$x = \left[\mathrm{r} + (i - r)\frac{\sin\beta}{\sin\theta}\right]\frac{\sin\theta}{\cos\beta}. \tag{4}$$

We can eliminate the angle β from this equation by noting that since twice the Bragg angle, 2θ, is the complement of the third angle of the triangle SCA whose other two angles are α and β, then

$$\beta = 2\theta - \alpha. \tag{5}$$

Similarly, we can eliminate the angle α by applying the law of sines to the triangle SCO with the angles α and $(\pi - \theta)$ opposite the sides r and $(r+s)$, respectively, to yield

$$\sin\alpha = \frac{r}{r+s}\sin\theta = f\sin\theta \tag{6}$$

where we have defined

$$f = r/(r+s). \tag{7}$$

Finally, the Bragg angle θ is related to the x-ray's wavelength λ and the energy E, as given in the main text above, by

$$\lambda = \frac{2d}{n}\sin\theta \quad \text{and} \quad E = \frac{hc}{\lambda} \tag{8}$$

where hc = 1.9864475 × 10^{-25} J·m (1.23984244 nm·keV) [22], d is the lattice spacing of the crystal, and n is the order of diffraction. Substituting Equations (5) through (8) into (3), expanding the trigonometric functions using standard trigonometric identities, and defining the variable

$$u \equiv \sin\theta = \frac{nhc}{2dE} \tag{9}$$

gives

$$x(E)=[r+(i-r)v]\frac{u}{w} \tag{10}$$

where

$$\begin{aligned} v &\equiv 2\sqrt{1-u^2}\sqrt{1-f^2u^2}-f(1-2u^2) \\ w &\equiv (1-2u^2)\sqrt{1-f^2u^2}+2fu^2\sqrt{1-u^2} \\ f &\equiv r/(r+s) \\ u &= E_0/E \\ E_0 &\equiv nhc/2d \end{aligned} \tag{11}$$

This result is exact for the ideal geometry described above and applies to the general case $i \neq r$. It is not clear that this relation can be analytically inverted to give $E(x)$, but it can in any case be numerically inverted to any accuracy required. An example of the dispersion relation $E(x)$ is shown in Figure 12(a) for the spectrometer shown in Figure 2, *i.e.* the case of a Si(111) crystal, which has a lattice spacing of $d = 0.3136$ nm in first order ($n = 1$), curved to a radius of $r = i = 150$ mm and with the source placed $s = 210$ mm from the crystal.

While equations 10 and 11 appear complex, when plotted in Figure 12(a) the smooth form of the dispersion function suggests the possibility of a simplifying approximation over limited energy ranges. Of the forms we have tested, the one that most closely matches the exact dispersion relation is:

$$E^2=\frac{a}{x^2}+b \tag{12}$$

where a and b are constants. Figure 12(b) plots the data in Figure 12(a) in terms of the variables E^2 and x^{-2}. The deviation from linearity is less that 1 eV. This suggests that a linear fit to calibration data plotted as E^2 against x^{-2} could provide a simple and practical spectrometer calibration scheme.

The constants a and b can be expressed in terms of the geometrical parameters of the spectrometer by the following method. Squaring both sides of Equation (10) gives a relationship between x^2 and u^2. Note that for the spectrometers discussed in this paper, the Bragg angle is small: $\theta < 0.1$ radians for typical spectrometer parameters and $E > 22$ keV. This implies $u^2 < 0.01$ and suggests making the power series expansion of x^2 in terms of u^2 about $u^2 = 0$. This series can in turn be written in terms of E^2 using Equation (9) above and can be inverted to give a power series for E^2 in terms of x^2 about $x^2 = 0$. The result is

$$E^2=ax^{-2}+b+\mathrm{O}\left[(x/r)^2\right] \tag{13}$$

where $\mathrm{O}\left[(x/r)^2\right]$ indicates the infinite number of additional terms of order $(x/r)^2$ and greater. The first two coefficients of the expansion are given by

$$\begin{aligned} a &= E_0^2 g^2 \\ b &= E_0^2 h/g \end{aligned} \tag{14}$$

where

$$\begin{aligned} g &\equiv r+(i-r)(2-f) \\ h &\equiv r(2-f)^2+(i-r)(6-8f+4f^2-f^3). \end{aligned} \tag{15}$$

After neglecting terms of order $(x/r)^2$ or greater one has equation (12) and can use this linear

relation to describe the dispersion relation to acceptable accuracy where the coefficients a and b can be determined either from the physical parameters of the spectrometer using Equations (14) and (15) or from a linear fit to calibration data plotted as E^2 as a function of x^{-2}. This approximation provides a useful inversion of the exact dispersion relation, Equation (10), to give E as a function of x. It can be used for initial spectrometer design and can also provide a good starting value for the numerical inversion of Equation (10).

FINAL REPORT BIBLIOGRAPHY

Publications from this work:

L. T. Hudson, R. D. Deslattes, A. Henins, C. T. Chantler, E. G. Kessler, and John E. Schweppe, "A curved crystal spectrometer for energy calibration and spectral characterization of mammographic x-ray sources," Medical Physics **23,** 1659-1670 (1996).

C. T. Chantler, R. D. Deslattes, A. Henins, and L. T. Hudson, "Flat and curved crystal spectrography for mammographic x-ray sources," Br. J. Radiol. **69**, 636-649 (1996).

Persons receiving pay from this work:

Dr. Richard D. Deslattes, NIST
Dr. Lawrence T. Hudson, NIST
Dr. Albert Henins, NIST

Meeting abstracts from this work:

[1] Invited talk at the American Association of Physicists in Medicine, Anaheim, CA 7/25-26/94 given by PI Richard D. Deslattes:

NON-INVASIVE AND SPECTRAL CHARACTERIZATION
OF MAMMOGRAPHIC X-RAY SOURCES

Mammographic sensitivity to kV choice and control is well established. While invasive high voltage divider procedures have the needed accuracy (when properly calibrated), they are somewhat inconvenient. Non-invasive techniques using differential filters offer exceptional convenience but are troubled by limited sensitivity and calibrations dependent both on target (and filtration) and the high voltage waveform. To improve this aspect of mammographic quality control, we have proposed a non-invasive technique based on wavelength dispersive diffraction spectrometry. In addition to providing direct access to accurate kV measurement, this approach gives the entire spectral distribution of the radiation produced by the source, its intrinsic filtration and any added filtration required by the mammographic technique.

[2] The same talk was given at a two-day workshop on traceability of dose and kV measurement at Physikallsch-Technische Bundesanstalt (PTB), Braunschweig, Germany on 9/11-12/94.